Studies of Meson-Meson Interactions within Lattice QCD

Ph.D. thesis

by

Attila Mihály

Kossuth Lajos University
Department of Theoretical Physics
Debrecen, 1998

Contents

Chapter 1

Introduction

Hadron-hadron interactions, in particular nucleon-nucleon interactions are of central importance in nuclear physics. The study of nuclei is a many-body problem which necessitates the solution of the Schrödinger equation with a given interaction potential. Therefore one of the most important tasks of theoretical nuclear physics is to find such a potential, from which the deuteron properties, the nucleon-nucleon scattering phase shifts, the properties of nuclear matter etc. — can be derived.

Eisenbud and Wigner [1] and later also Okubo and Marshak [2] pointed out that the nucleon-nucleon potential must fulfill general requirements from the fundamental conservation laws. Demanding invariance under space-time translations, Galilei transformations, rotations, time and space inversion, and further on an approximate charge symmetry, they set up a general non-relativistic, hermitian nucleon-nucleon potential. This potential includes central, spin-spin, tensor, spin-orbit and quadratic spin-orbit terms. The determination of the coefficients of these terms leads to phenomenological potentials, such as the Reid potential [3].

A somewhat more fundamental derivation of the nucleon-nucleon potential is possible within models assuming mesons and baryons as fundamental degrees of freedom. Here, the interactions between baryons are mediated by exchange of mesons. For example, the Bonn potential [4–6] is obtained from a field-theoretical Hamiltonian, containing nucleon-nucleon-meson and nucleon-Δ-meson interaction vertices. In the Paris model [7] nucleon-pion and pion-pion interactions are considered, but all contributions to the interaction are directly derived from experiment and not calculated within a field theory.

Nowadays it is generally accepted that hadrons are composite particles. To systematize the numerous hadron states, in 1963 Gell-Mann proposed that mesons should be thought of being composites of a quark and an anti-quark, whereas baryons should consist of three quarks. In this way all known hadrons could be built up, and the model could also predict the existence of a new hadron, called Ω^-, which was discovered one year later. There is also experimental evidence for the existence of hadronic substructure. The average hadron radius is of the order of 1 fm. Deep inelastic lepton-hadron scattering indicated the existence of scattering centers with an extent of less than 10^{-3} fm. From the scattering angular distribution observed in these experiments the spin of the constituents was determined to be $1/2\hbar$. Their charge turned out to be a fraction (+2/3 or –1/3) of the unit charge. Nevertheless, up to now all attempts to isolate a single quark experimentally have failed. The quarks are apparently enclosed in the hadrons. This phenomenon is called quark confinement.

The quark potential models of hadron-hadron interactions take the compositeness of hadrons into account. A typical example is the non-relativistic model of Isgur et al. [8]. Here, one tries to derive an effective nucleon-nucleon potential via variational calculations with a six-quark wave-function and a Hamiltonian, in analogy with the variational techniques used for the hydrogen molecule in atomic physics. A relativistic approach to the nucleon-nucleon interaction is the bag model [9]. Examples of bag models are the MIT-bag [10], the little-bag [11] and the cloudy-bag model [12]. A common feature of quark potential and bag models is that quark confinement is imposed artificially on the system by an additional constraint.

All afore mentioned models contain parameters to fit the results to experiments. They usually yield a good quantitative outcome within a certain energy range, but from their very construction, a fundamental understanding of the nuclear interaction cannot be obtained.

The correct theory to describe the interaction between quarks is believed to be Quantum Chromodynamics (QCD). In this theory the interactions between quarks are the result of the exchange of vector particles called gluons. Encouraged by the great success of Quantum Electrodynamics (QED), and as an attempt for a generalized treatment of different interactions, QCD was formulated as a quantum field theory based on the principle of local gauge invariance. In contrast to QED, which is an Abelian theory, QCD is formulated as a non-Abelian gauge field theory based on the group SU(3). This choice of the gauge group was suggested by the antisymmetrization procedure of the three-quark system. As a consequence the fields carry an

additional quantum number, called color. Quark fields transform according to the fundamental representation of SU(3). All hadrons transform as color singlets, and are therefore called "color neutral". Because of the non-Abelian structure the colored gluons can couple to themselves. These self couplings, one believes, are responsible for quark confinement. Nevertheless, the connection between confinement and non-Abelian fields is not yet totally understood.

QCD is an asymptotically free theory, i.e. the coupling constant is small for large four-momentum transfer [13, 14]. At low energies, however, the coupling constant becomes large. Consequently, perturbation theory does not work in the low energy regime. Therefore the calculation of phenomena at nucleonic distances requires non-perturbative tools. The interest in non-perturbative methods for a fundamental treatment of QCD low energy phenomena led to the formulation of QCD on the lattice [15]. Here, quarks are defined on the sites of a fictitious four-dimensional space-time lattice, whereas gauge fields are placed on the links between the sites. The formulation of the theory as a path integral in euclidean space-time leads to an analogy between the field theoretical vacuum expectation value and the partition function in statistical mechanics. In this way, within field theories one can apply the well-known tools of statistical mechanics, such as analytical series expansions or numerical Monte Carlo simulations. Furthermore, the use of a lattice represents the introduction of a regularization scheme for the quantum field theory. The momenta are restricted to the first Brillouin zone, therefore high momenta are cut off and consequently ultraviolet divergences are removed. To obtain physically relevant results from a lattice calculation one has to perform the continuum limit, that is the limit of infinitesimally small lattice constants. The practical approach of the continuum limit still poses a difficult problem. A short overview about the basics of lattice QCD is given in Chapter 2. More detailed descriptions can be found in the standard textbooks of M. Creutz [16], H.J. Rothe [17] and I. Montvay and G. Münster [18].

Within the framework of QCD, the hadron-hadron interactions are residual forces between two quark clusters, each consisting of two or three quarks (mesons and baryons, respectively). The hadron-hadron forces are mediated for short distances by gluon exchange between the constituent quarks whereas for longer distances the production of quark-antiquark pairs is expected to be the dominating mechanism, which can be interpreted as an effective meson exchange. This explains why the meson exchange potentials give a satisfactory description of nucleon-nucleon scattering for long

distances, whereas quark potential and bag models are mainly successful for short distances. Remarkably, only few attempts have been made to extract effective interactions, or potentials, between two composite hadrons in the framework of a lattice discretized theory [19–22]. This task is very challenging since the residual interaction between two color singlets is about 10^{-2} to 10^{-3} times smaller than a typical hadron mass.

This work is an attempt to obtain hadron-hadron potentials in the framework of lattice QCD. As a simplification, the interaction between two hadrons consisting of a heavy and a light quark degree of freedom (K, B, D mesons) is investigated. Different aspects of this problem are presented in Chapter 3. Section 3.1 is devoted to the definition and simulation of quark propagators on the lattice, being the key quantities of our investigation. The Green functions describing the dynamics of the one-meson and two-meson systems are constructed in Section 3.2. The heavy-light approximation and the interaction potentials between two heavy-light color singlets for various light-quark mass parameter are presented in Section 3.3. In Section 3.4, potentials between a heavy-light meson and the corresponding antiparticle are computed. A lattice improvement technique allowing for a refined analysis as well as the simulation results obtained by this technique are presented in Section 3.5. Finally, Chapter 4 is for the summary and outlook.

Chapter 2

Lattice Quantum Chromodynamics

2.1 QCD Lagrangian

Nowadays it is generally accepted that the theory for strong interactions should be Quantum Chromodynamics, since in the domain of high energy scattering QCD is highly successful. QCD was constructed along the lines of the very successful Quantum Electrodynamics (QED) as a quantized gauge field theory with a local gauge symmetry. In contrast to the Abelian U(1) gauge symmetry of QED, the QCD Lagrangian is invariant under non-Abelian SU(3) gauge transformations. Whereas in QED electrons and photons are the fundamental particles, in QCD quarks and gluons are the basic degrees of freedom. Quarks are fermionic matter fields. They transform according to the fundamental triplet representations of $\mathrm{SU}(3)_{\mathrm{color}}$. Gluons are bosonic gauge fields and transform according to the octet representation. The QCD Lagrangian consists of a gluonic and a fermionic part,

$$\begin{aligned} \mathcal{L}^{\mathrm{QCD}} &= \mathcal{L}_{\mathrm{G}}^{\mathrm{QCD}} + \mathcal{L}_{\mathrm{F}}^{\mathrm{QCD}} \\ &= -\frac{1}{4} F^a_{\mu\nu}(x) F_a^{\mu\nu}(x) + \sum_{f=1}^{n_f} \bar{\psi}_f(x)(i\not{D} - m_f)\psi_f(x) \ , \end{aligned} \tag{2.1}$$

where ψ_f is the Dirac spinor, m_f the quark mass and n_f the number of flavors. The generalized field strength tensor $F_a^{\mu\nu}(x)$ is

$$F_a^{\mu\nu}(x) = \partial^\mu A_a^\nu(x) - \partial^\nu A_a^\mu(x) - g f_{abc} A_b^\mu(x) A_c^\nu(x) \ , \tag{2.2}$$

where $a, b, c = 1, \ldots, 8$ are SU(3) indices. A_a^μ is the gauge field, g is the coupling constant, and f_{abc} are the structure constants of SU(3). $\not{D}$ is an abbreviation for $\gamma_\mu D^\mu(x)$, where

$$D^\mu(x) = \partial^\mu + igA_a^\mu(x)\frac{\lambda^a}{2} \tag{2.3}$$

is the gauge covariant derivative with the generators λ_a of SU(3) (Gell-Mann matrices).

The Lagrangian (2.1) allows for the formulation of QCD as a quantum field theory. One possible quantization is the path integral formulation of QCD.

2.2 Path Integral Approach to Quantization

Since its introduction by Feynman [23] the path integral method has become a very important tool for elementary particle physicists. Many of the modern developments in theoretical particle physics are based on this method. One of these developments is the lattice formulation of field theories. In contrast to classical mechanics, in quantum mechanics the exact trajectory of a particle in configuration space is not known; instead, one has to calculate transition amplitudes like

$$\langle\, q_t' \,|\, q_{t_0} \,\rangle \;, \tag{2.4}$$

where $|\, q_{t_0} \,\rangle$ and $|\, q_t' \,\rangle$ are eigenstates of the space coordinate operator $Q(t)$ in the Heisenberg picture. The absolute square of the transition amplitude (2.4) is proportional to the probability that a particle which at the time t_0 was located at q, at the time t will be found at q'.

There exist infinitely many paths connecting the initial point with the final one. Feynman showed [24] that the transition amplitude (2.4) can be found by integrating over all possible paths, weighted with the phase factor $\exp(iS[q])$, where

$$S[q] = \int_{t_0}^{t} dt'\, L(q(t'), \dot{q}(t')) \tag{2.5}$$

is the classical action. This prescription can be symbolically written in terms of a functional or path integral:

$$\langle\, q_t' \,|\, q_{t_0} \,\rangle = \int_q^{q'} \mathcal{D}[q] e^{iS[q]} \;. \tag{2.6}$$

Notice that while the canonical quantization goes far away from the original formulation of classical mechanics, the path integral representation of Feynman reestablishes the connection with the classical action principle. The function weighting the paths is actually $\exp(iS[q]/\hbar)$. In the limit $\hbar \to 0$ this is a rapidly oscillating function. As a consequence, the contribution of all paths to the transition amplitude (2.4) vanishes, except that of the path for which $\delta S[q] = 0$. This is the principle of least action which leads to the classical equations of motion. Thus, within the path integral framework the quantization of a classical system amounts to taking into account fluctuations around the classical path.

As a possible way of quantization, the path integral formalism can be also introduced in field theories. Within QCD the vacuum expectation value of an operator is calculated according to

$$\langle\, O \,\rangle = \langle\, 0 \,|\, O \,|\, 0 \,\rangle = \frac{1}{Z} \int \mathcal{D}[A]\ \mathcal{D}[\psi]\ \mathcal{D}[\bar{\psi}]\ e^{iS[A,\psi,\bar{\psi}]}\ O(A,\psi,\bar{\psi})\ , \qquad (2.7)$$

with the vacuum-to-vacuum transition amplitude

$$\langle\, 0 \,|\, 0 \,\rangle \equiv Z = \int \mathcal{D}[A]\ \mathcal{D}[\psi]\ \mathcal{D}[\bar{\psi}]\ e^{iS[A,\psi,\bar{\psi}]}\ . \qquad (2.8)$$

Here the functional integration extends over all gauge field configurations $A^\mu_a(x)$ (Lorentz index $\mu = 0,\ldots,3$, group index $a = 1,\ldots,8$) and over all configurations of the fermionic fields $\psi^\alpha_c(x)$ and $\bar{\psi}^\alpha_c(x)$ (spinor index $\alpha = 1,\ldots,4$, color index $c = 1,2,3$). Because of the anti-commutation relations of the fermionic fields these are represented by Grassmann variables.

Since the weights in (2.7) and (2.8) are oscillating functions, this path integral representation is not suited for numerical calculations. The problem can be overcome by formulating QCD on a four-dimensional euclidean space. This is achieved by an analytical continuation to imaginary time

$$t = x_0 \to -ix_4 \qquad \text{with real } x_4\ . \qquad (2.9)$$

The transition to the euclidean space from the Minkowski space can be done by using in the formulae the replacement (2.9) whenever t appears explicitly, together with the proper replacement of the four-component quantities with those valid in the euclidean space. In QCD, three such replacements should be performed: $\partial_0 \to i\partial_4$, $p_0 \to ip_4$, and $A_0 \to iA_4$. Thus, for the euclidean gluonic Lagrangian $\mathcal{L}^{\rm E}_{\rm G}$ one obtains:

$$\mathcal{L}^{\rm M}_{\rm G} \quad = \quad -\frac{1}{4} F^a_{\alpha\beta}(x) F^{\alpha\beta}_a(x)$$

$$\begin{aligned} &= -\frac{1}{4}\Big(F^a_{ij}(x)F^a_{ij}(x) - 2F^a_{0j}(x)F^a_{0j}(x) + F^a_{00}(x)F^a_{00}(x)\Big) \\ &\to -\frac{1}{4}\Big(F^a_{ij}(x)F^a_{ij}(x) + 2F^a_{4j}(x)F^a_{4j}(x) + F^a_{44}(x)F^a_{44}(x)\Big) \\ &= -\frac{1}{4}F^a_{\mu\nu}(x)F^a_{\mu\nu}(x) \equiv -\mathcal{L}^{\mathrm{E}}_{\mathrm{G}} \ . \end{aligned} \tag{2.10}$$

Here, $\alpha, \beta = 0, \ldots, 3$ are four indices in Minkowski space, and $\mu, \nu = 1, \ldots, 4$ are those in Euclidean space. For the fermionic Lagrangian one obtains

$$\mathcal{L}^{\mathrm{M}}_{\mathrm{F}} = \bar{\psi}(x)(i\not{D} - m)\psi(x) \to -\bar{\psi}(x)(D_\mu\gamma_\mu + m)\psi(x) \equiv -\mathcal{L}^{\mathrm{E}}_{\mathrm{F}} \ . \tag{2.11}$$

The euclidean γ matrices fulfil the anti-commutation relations

$$\{\gamma_\mu, \gamma_\nu\} = 2\delta_{\mu\nu} \ . \tag{2.12}$$

A possible choice for the γ matrices is

$$\gamma_4 = \begin{pmatrix} 1 & 0 \\ 0 & -1 \end{pmatrix} \ , \qquad \gamma_i = \begin{pmatrix} 0 & \sigma_i \\ \sigma_i & 0 \end{pmatrix} \ , \tag{2.13}$$

with the Pauli matrices σ_i. They are hermitian, i.e.

$$\gamma_\mu = \gamma_\mu^\dagger \ . \tag{2.14}$$

With $i\int dx_0 = \int dx_4$ one obtains the complete euclidean action

$$\begin{aligned} iS^{\mathrm{M}} &= i\int d^4x \ (\mathcal{L}^{\mathrm{M}}_{\mathrm{G}} + \mathcal{L}^{\mathrm{M}}_{\mathrm{F}}) = i\int dx_0 \ d^3x \ (\mathcal{L}^{\mathrm{M}}_{\mathrm{G}} + \mathcal{L}^{\mathrm{M}}_{\mathrm{F}}) \\ &\to \int dx_4 \ d^3x \ (-\mathcal{L}^{\mathrm{E}}_{\mathrm{G}} - \mathcal{L}^{\mathrm{E}}_{\mathrm{F}}) \equiv -S^{\mathrm{E}} \ . \end{aligned} \tag{2.15}$$

The vacuum expectation value of an observable in the euclidean path integral formulation is therefore

$$\langle\, O \,\rangle \ = \frac{1}{Z} \int \mathcal{D}[A] \ \mathcal{D}[\psi] \ \mathcal{D}[\bar{\psi}] \ e^{-S^{\mathrm{E}}[A,\psi,\bar{\psi}]} \ O(A,\psi,\bar{\psi}) \ , \tag{2.16}$$

with

$$Z = \int \mathcal{D}[A] \ \mathcal{D}[\psi] \ \mathcal{D}[\bar{\psi}] \ e^{-S^{\mathrm{E}}[A,\psi,\bar{\psi}]} \ . \tag{2.17}$$

If the system is periodic in euclidean time, then Z can be viewed as a partition function and (2.16) has the form of a statistical ensemble average with a Boltzmann distribution given by $\exp(-S^{\mathrm{E}}[A,\psi,\bar{\psi}])$. This allows us

to use well-known statistical methods to calculate expectation values. The non-perturbative studies of QCD are based on this simple observation.

Results from the euclidean space should in principle be analytically continued back to Minkowski space. For many physical problems, however, like the calculation of the mass of a particle from the asymptotic behavior of its propagator one can obtain results directly from the euclidean formulation.

2.3 Lattice Regularization

As we have seen in the previous section, formulating QCD in the euclidean space-time opens up the possibility for numerical calculations. But since the fields A, ψ and $\bar{\psi}$ have infinite degrees of freedom, at each coordinate $x = (x_1, x_2, x_3, x_4)$, the integration measure $\mathcal{D}[A, \psi, \bar{\psi}]$ is still mathematically not well defined. To give the path integrals a precise meaning, one discretizes both time and space, i.e. introduces a space-time lattice, and restricts x to a multiple of a "lattice spacing" a, i.e. $x = na$, with n an integer. Defining the fields on this euclidean space-time lattice one obtains a discrete set of variables. The functional integration over all field configurations simplifies to an integration over these variables.

The Fourier transform of a function $f(x)$ defined on the periodic lattice

$$\tilde{f}(p) = a^4 \sum_x e^{ipx} f(x) \tag{2.18}$$

is periodic in p with the period $p_\mu = 2\pi/a$. Therefore momentum is restricted to the first Brillouin zone $-\pi/a < p_\mu \leq \pi/a$. This removes ultraviolet divergences. So the introduction of a lattice provides a regularization scheme.

Internal symmetries survive discretization whereas spatial symmetries are broken. This is obvious for the euclidean Poincaré group, which contains O(4) rotations, but on the lattice only rotations by multiples of $\pi/2$ are allowed. The enormous advantage is that local gauge invariance can be preserved. Furthermore, in the limit $a \to 0$ one should recover the continuum theory. However, there is no unique choice of a discrete action fulfilling this requirement.

2.4 Fermions on the Lattice

2.4.1 Species Doubling

While scalar and vector fields can be simply assigned to the sites of the lattice, the gauge fields neccessitate a careful treatment, in order to preserve gauge invariance. The association of spinors to the lattice is even more difficult and not yet satisfactorily solved.

The euclidean free fermionic continuum action is

$$S_{\mathrm{F}} = \int d^4x \ \bar{\psi}(x)(\partial_\mu \gamma_\mu + m)\psi(x) \ . \tag{2.19}$$

Following the naive discretization scheme we introduce a four dimensional space-time lattice. With each site x of the lattice we associate an independent four-component spinor variable ψ_x. To keep the action simple, we replace the derivative by a symmetric differential quotient:

$$\partial_\mu \psi_x \to \frac{1}{2a}[\psi_{x+\hat{\mu}} - \psi_{x-\hat{\mu}}] \ . \tag{2.20}$$

Substituting $\int d^4x$ by $a^4 \sum_x$ we arrive at the following free fermionic discretized action [25]:

$$S_{\mathrm{F}} = a^4 \Big\{ \frac{1}{2a} \sum_{x,\mu} \Big[\bar{\psi}_x \gamma_\mu \psi_{x+\hat{\mu}} - \bar{\psi}_{x+\hat{\mu}} \gamma_\mu \psi_x \Big] + m \sum_x \bar{\psi}_x \psi_x \Big\} \ . \tag{2.21}$$

Contrary to expectations, the above action does not reproduce the correct continuum limit, because it has a new hidden degeneracy in the fermionic degrees of freedom. To see this let us consider the propagator of a massless free fermion in momentum space

$$G(p) = \frac{1}{\frac{1}{a} \sum_\mu \gamma_\mu \sin(p_\mu a)} \ . \tag{2.22}$$

Besides the physical pole at $p_\mu a = 0$ there are 15 further poles in the first Brillouin zone at

$$p_\mu a = (\pi,0,0,0) \ , (0,\pi,0,0) \ , \ldots , (\pi,\pi,0,0) \ , \ldots , (\pi,\pi,\pi,\pi) \ . \tag{2.23}$$

Thus the naively discretized action describes 16 fermions and consequently cannot reproduce the original continuum Lagrange density in the limit $a \to 0$. This proliferation of fermions is called fermion doubling.

Fermion doubling is a fundamental problem for all lattice actions that preserve the chiral symmetry in the massless continuum limit. It can be shown that it is impossible to construct a chirally invariant lattice action that is free of degeneracy. A chirally symmetric lattice fermion action is at least four-fold degenerate [26, 27]. One has the choice of an action that is not degenerate in the number of fermions but breaks chiral symmetry explicitly for a finite lattice constant. This is achieved with the Wilson method [15]. The second possibility is to preserve chiral invariance at least partly and to accept a partial fermion degeneracy, like in the Kogut-Susskind method [28, 29].

2.4.2 Wilson Fermions

Wilson's idea was to modify the action (2.21) in such a way that the zeros of the denominator in (2.22) at the edges of the Brillouin zone are lifted by an amount proportional to the inverse lattice spacing. This is achieved by adding an extra term

$$ra^4 \sum_x \sum_\mu \frac{1}{2a} \; (\bar{\psi}_{x+\hat{\mu}} - \bar{\psi}_x)(\psi_{x+\hat{\mu}} - \psi_x) \; , \tag{2.24}$$

where $0 < r \leq 1$ is a free parameter [15, 25]. This term is of order a^5:

$$ra^4 \sum_x \sum_\mu \frac{1}{2a} \; a\bar{\psi}'_x \; a\psi'_x \; \sim \; O(a^5) \; , \tag{2.25}$$

and vanishes in the classical continuum limit, relative to the rest of the action, which is of order a^4.

The new action becomes

$$\begin{aligned} S_{\rm F} = a^4 \Big\{ \frac{1}{2a} \sum_{x\mu} \Big(& \bar{\psi}_x \gamma_\mu \psi_{x+\hat{\mu}} - \bar{\psi}_{x+\hat{\mu}} \gamma_\mu \psi_x + r\bar{\psi}_{x+\hat{\mu}} \psi_{x+\hat{\mu}} + \\ & r\bar{\psi}_x \psi_x - r\bar{\psi}_{x+\hat{\mu}} \psi_x - r\bar{\psi}_x \psi_{x+\hat{\mu}} \Big) + m \sum_x \bar{\psi}_x \psi_x \Big\} \; . \end{aligned} \tag{2.26}$$

Using

$$\begin{aligned} \frac{1}{2a} \sum_x \sum_\mu \bar{\psi}_x \psi_x &= \frac{2}{a} \sum_x \bar{\psi}_x \psi_x \; , \\ \frac{1}{2a} \sum_x \sum_\mu \bar{\psi}_{x+\hat{\mu}} \psi_{x+\hat{\mu}} &= \frac{2}{a} \sum_x \bar{\psi}_x \psi_x \; , \end{aligned} \tag{2.27}$$

and rescaling the fields

$$\begin{aligned} \psi &\rightarrow \left[a^3(4r+ma)\right]^{-1/2}\ \psi\ , \\ \bar{\psi} &\rightarrow \left[a^3(4r+ma)\right]^{-1/2}\ \bar{\psi}\ , \end{aligned} \tag{2.28}$$

one obtains

$$S_{\mathrm{F}} = -\kappa \sum_{x,\mu} \left[\bar{\psi}_x(r-\gamma_\mu)\psi_{x+\hat{\mu}} + \bar{\psi}_{x+\hat{\mu}}(r+\gamma_\mu)\psi_x\right] + \sum_x \bar{\psi}_x\psi_x\ , \tag{2.29}$$

with the hopping parameter

$$\kappa = \frac{1}{8r+2ma}\ . \tag{2.30}$$

Defining the fermionic matrix

$$M_{xx'} = \delta_{xx'} - \kappa\ Q_{xx'} \tag{2.31}$$

with

$$Q_{xx'} = \sum_\mu \left[(r-\gamma_\mu)\ \delta_{x+\hat{\mu},x'} + (r+\gamma_\mu)\ \delta_{x,x'+\hat{\mu}}\right]\ , \tag{2.32}$$

the corresponding fermion propagator turns out to be

$$G(p) = \widetilde{M}^{-1}(p) \propto \frac{1}{m + \frac{i}{a}\sum_\mu \sin(p_\mu a) + \frac{r}{a}\sum_\mu (1-\cos(p_\mu a))}\ . \tag{2.33}$$

The originally degenerate particles acquire an additional mass on the former poles from the Wilson term

$$p_\mu a = \begin{cases} (\pi,0,0,0)\ ,\ldots,\ (0,0,0,\pi) & m+2r/a \\ (\pi,\pi,0,0)\ ,\ldots,\ (0,0,\pi,\pi) & m+4r/a \\ (\pi,\pi,\pi,0)\ ,\ldots,\ (0,\pi,\pi,\pi) & m+6r/a \\ (\pi,\pi,\pi,\pi) & m+8r/a\ . \end{cases} \tag{2.34}$$

These states have an infinite mass in the limit $a \rightarrow 0$ and disappear from the spectrum. The degeneracy is completely removed.

The diagonal parts of the Wilson term correspond to an additional mass term, which breaks the chiral symmetry explicitly. This means that even for $m = 0$ the Lagrangian is not invariant under chiral transformations. The additional mass term also gives rise to mass counter terms in the renormalization process. Therefore, a vanishing bare mass m_0 does not generally lead to a renormalized mass $m_{\mathrm{ren}} = 0$.

2.4.3 Kogut-Susskind Fermions

As we have seen above, the fermion doubling problem owes its existence to the fact that the propagator (2.22) has extra poles at the edges of the Brillouin zone. This suggests the possibility of eliminating the unwanted fermion modes by reducing the Brillouin zone. This can be accomplished by distributing the components of a spinor over a unit cube instead of defining it on a single lattice point. In this way the corresponding components of two spinors are separated by two fundamental lattice spacings and therefore the first Brillouin zone reduces to $-\pi/2a \leq p_\mu \leq \pi/2a$ so that the pole at π/a is outside. Since in d space-time dimensions there are 2^d sites within a hypercube, but e.g. only $2^{d/2}$ components of a Dirac spinor for d-even, one needs extra Dirac fields to reduce the Brillouin zone by a factor of two. In four space-time dimensions such a prescription may therefore be appropriate for describing $2^2 = 4$ different flavors of quarks, degenerate in mass. Thus the degeneracy is not completely lifted, it is only reduced to four.

An illustrative way to arrive at the definition of staggered fermions is the so-called spin diagonalization, which consists in performing a local change of variables

$$\begin{aligned} \psi_x &= A_x \chi_x \ , \\ \bar{\psi}_x &= \bar{\chi}_x A_x^\dagger \ . \end{aligned} \tag{2.35}$$

The transformation matrix A_x is a unitary matrix diagonalizing all the γ-matrices in the action in the sense that

$$A_x^\dagger \gamma_\mu A_{x+\hat{\mu}} = \Delta_{x\mu} \ , \tag{2.36}$$

where $\Delta_{x\mu}$ is proportional to the unity matrix, i.e.

$$\Delta_{x\mu} = \Gamma_{x\mu} \ 1 \ . \tag{2.37}$$

There exist different solutions for A_x, for instance,

$$A_x = \gamma_1^{x_1} \gamma_2^{x_2} \gamma_3^{x_3} \gamma_4^{x_4} \ , \tag{2.38}$$

where the integers x_1, x_2, x_3, x_4 are components of the lattice site four-vector x. In this case one gets

$$\Gamma_{x\mu} \ = \ (-1)^{x_1 + \ldots + x_{\mu-1}} \quad (\mu = 1, 2, 3, 4) \ . \tag{2.39}$$

In terms of the new fields χ_x, $\bar{\chi}_x$ the naive action (2.21) becomes

$$S_{\mathrm{F}} = a^4 \left\{ \frac{1}{2a} \sum_{x,\mu} \left[\bar{\chi}_x \Delta_{x\mu} \chi_{x+\hat{\mu}} - \bar{\chi}_{x+\hat{\mu}} \Delta^{\dagger}_{x\mu} \chi_x \right] + m \sum_x \bar{\chi}_x \chi_x \right\} . \qquad (2.40)$$

Since this is diagonal in the Dirac indices, the different components can be decoupled, and one can reduce the number of fermion field components obtaining the following free Kogut-Susskind, or staggered fermionic action:

$$S_{\mathrm{F}} = a^4 \left\{ \frac{1}{2a} \sum_{x,\mu} \Gamma_{x\mu} \left[\bar{\chi}_x \chi_{x+\hat{\mu}} - \bar{\chi}_{x+\hat{\mu}} \chi_x \right] + m \sum_x \bar{\chi}_x \chi_x \right\} . \qquad (2.41)$$

Now χ_x and $\bar{\chi}_x$ are one component fermion fields. The reduction of the number of degrees of freedom by a factor of four leads, instead of the 16 naive fermion species, to four degenerate species in the staggered fermion action. They might be interpreted as four 'flavors' of fermions. One can formally remove this remaining degeneracy and introduce an arbitrary number of components by multiplying with a scale factor f describing $4f$ flavors of Dirac fermions.

For $m = 0$ the reduced action is invariant with respect to the global transformations

$$\left.\begin{array}{l} \chi_x \to e^{i\alpha} \chi_x \\ \bar{\chi}_x \to e^{-i\beta} \bar{\chi}_x \end{array}\right\} \text{for } (-1)^{x_1+x_2+x_3+x_4} = \quad 1$$

$$\left.\begin{array}{l} \chi_x \to e^{i\beta} \chi_x \\ \bar{\chi}_x \to e^{-i\alpha} \bar{\chi}_x \end{array}\right\} \text{for } (-1)^{x_1+x_2+x_3+x_4} = -1 , \qquad (2.42)$$

where α and β are independent phases. This residual symmetry originates from the chiral symmetry of the continuum action and ensures that no counter terms are needed for renormalization (that means $m_{\mathrm{bare}} = 0$ implies $m_{\mathrm{ren}} = 0$). This is a fundamental difference to the Wilson method. As a consequence the non-renormalized mass parameter in the staggered action and the bare mass in the hopping parameter of the Wilson action are not identical. Therefore a direct comparison of the two methods is not easy to accomplish.

In the Kogut-Susskind formulation of lattice fermions baryonic operators with well defined quantum numbers are difficult to construct. Thus the Wilson formalism is more adequate for hadron spectroscopy purposes. Since chiral symmetry is partially conserved, the staggered scheme is attractive for studying questions like spontaneous symmetry breaking in QCD. The

price one has to pay is that the degeneracy cannot be completely avoided, for reasons mentioned in Section 2.4.1. In practice one introduces a factor $f = 1/4$ in the action to account for the remaining degeneracy. Whether this concept gives the correct continuum limit is an unsolved problem.

2.5 Pure and Full Lattice QCD Action

The lattice regularization of gauge fields should be performed by preserving gauge invariance. One can easily verify that a naive discretization by simply assigning the vector potentials to the sites and substituting all derivatives with finite differential quotients would violate local gauge invariance for finite lattice spacing a.

The gluonic fields were introduced in the Dirac part of the continuum QCD Lagrangian (2.1) by demanding invariance of the fermionic action with respect to the SU(3) gauge transformations, and adding a gauge-invariant kinetic term. The definition of the gauge fields on the lattice can be obtained by following this procedure. Let us consider the free fermionic discretized action (2.21), where the fields ψ_x and $\bar{\psi}_x$ are now three-component fields in color space (being also four-component spinor variables) so that the Lagrangian is invariant under the global transformations

$$\begin{aligned} \psi_x &\rightarrow g\psi_x \\ \bar{\psi}_x &\rightarrow \bar{\psi}_x g^{-1}\,, \end{aligned} \tag{2.43}$$

where g is an element of SU(3). The next step consists in requiring the theory to be invariant under local SU(3) transformations, with the group element g_x depending on the lattice site. For this, one has to make the following substitutions in (2.21):

$$\begin{aligned} \bar{\psi}_x \psi_{x+\hat{\mu}} &\rightarrow \bar{\psi}_x U_{x\mu} \psi_{x+\hat{\mu}} \\ \bar{\psi}_{x+\hat{\mu}} \psi_x &\rightarrow \bar{\psi}_{x+\hat{\mu}} U_{x+\hat{\mu},-\mu} \psi_x\ . \end{aligned} \tag{2.44}$$

The factors $U_{x\mu}$ and $U_{x+\hat{\mu},-\mu}$ are determined by the line integral of A_μ along the link, e.g.

$$U_{x\mu} \equiv \mathrm{P}\ \exp\left(-i \int_x^{x+a\hat{\mu}} g A_\mu \cdot dy\right)\ , \tag{2.45}$$

where the P-operator path-orders the A_μ's along the integration path. Notice that $U_{x\mu}$ and $U_{x+\hat{\mu},-\mu}$ are elements of the SU(3) group, transforming

according to

$$\begin{aligned} U_{x\mu} &\rightarrow g_x U_{x\mu} g^{-1}_{x+\hat{\mu}} \\ U_{x+\hat{\mu},-\mu} &\rightarrow g_{x+\hat{\mu}} U_{x+\hat{\mu},-\mu} g^{-1}_x \ , \end{aligned} \tag{2.46}$$

and satisfying the relation

$$U_{x+\hat{\mu},-\mu} = U^\dagger_{x\mu} = U^{-1}_{x\mu} \ . \tag{2.47}$$

In contrast to the matter fields, the group elements $U_{x\mu}$ live on the links connecting two neighboring lattice sites; hence, they are referred to as "link variables".

Making the substitutions (2.44) in eq. (2.21), we obtain the following gauge-invariant lattice fermionic action:

$$S_{\rm F} = a^4 \left\{ \frac{1}{2a} \sum_{x,\mu} \left[\bar{\psi}_x \gamma_\mu U_{x\mu} \psi_{x+\hat{\mu}} - \bar{\psi}_{x+\hat{\mu}} \gamma_\mu U^\dagger_{x\mu} \psi_x \right] + m \sum_x \bar{\psi}_x \psi_x \right\} . \tag{2.48}$$

In this formula the color, Dirac and flavor indices are omitted. Using (2.45), $S_{\rm F}$ yields formally the correct continuum limit:

$$S_{\rm F} \stackrel{a\rightarrow 0}{\longrightarrow} \int d^4x \ \bar{\psi}(x)(D_\mu \gamma_\mu + m)\psi(x) \ . \tag{2.49}$$

The change of (2.48) to the Wilson and staggered fermionic actions (2.29) and (2.41) is obvious. In the staggered scheme the fields ψ become three-component vectors χ in color space and should be coupled to the matrix-valued link variables in the same gauge-invariant way. The gauge-invariant staggered fermionic action reads:

$$S_{\rm F} = a^4 \left\{ \frac{1}{2a} \sum_{x,\mu} \Gamma_{x\mu} \left[\bar{\chi}_x U_{x\mu} \chi_{x+\hat{\mu}} - \bar{\chi}_{x+\hat{\mu}} U^\dagger_{x\mu} \chi_x \right] + m \sum_x \bar{\chi}_x \chi_x \right\} . \tag{2.50}$$

It can be rewritten in terms of dimensionless lattice variables, by making the replacements

$$\begin{aligned} m &\rightarrow \frac{1}{a} m \ , \\ \bar{\chi}_x &\rightarrow \frac{1}{a^{3/2}} \bar{\chi}_x \ , \\ \chi_x &\rightarrow \frac{1}{a^{3/2}} \chi_x \ . \end{aligned} \tag{2.51}$$

Then the lattice version of (2.50) applicable in computer codes is

$$S_{\rm F} = \sum_{x,\mu} \frac{1}{2}\Gamma_{x\mu}\Big[\bar{\chi}_x U_{x\mu}\chi_{x+\hat{\mu}} - \bar{\chi}_{x+\hat{\mu}}U^\dagger_{x\mu}\chi_x\Big] + m\sum_x \bar{\chi}_x\chi_x \ . \tag{2.52}$$

The lattice form of the gluonic Lagrange density should also be gauge invariant. There is no unique way of constructing the lattice Lagrangian but it has to converge to the continuum Lagrangian for $a \to 0$. Since $U_{x\mu}$ transforms according to (2.46), the simplest gauge-invariant quantity one can build from the group elements $U_{x\mu}$, is the trace of the path ordered product of link variables along the boundary of an elementary plaquette:

$$U_{{\rm pl},\mu\nu}(x) = U_{x\mu}U_{x+\hat{\mu},\nu}U^\dagger_{x+\hat{\nu},\mu}U^\dagger_{x\nu} \ . \tag{2.53}$$

The gauge invariant expression [15]

$$S_{\rm G} = \beta \sum_{\rm pl}\Big(1 - \frac{1}{3}\,{\rm Re}\,{\rm Tr}\,U_{\rm pl}\Big) \ , \tag{2.54}$$

with the inverse coupling constant $\beta = 6/g^2$, and the sum extending over all distinct plaquettes on the lattice, converges to the continuum action for $a \to 0$

$$S_{\rm G} \stackrel{a\to 0}{\longrightarrow} \int d^4x \ \frac{1}{4}F_{\mu\nu}(x)F_{\mu\nu}(x) \ . \tag{2.55}$$

Thus the action (2.54) — referred to as the Wilson plaquette action — is one possible choice of the gluonic action on the lattice. Together with the action (2.50) we now have a gauge-invariant lattice regularized version of QCD.

The persistence of the exact gauge invariance has several practical advantages. With gauge invariance, the quark-gluon, three-gluon, and four-gluon coupling constants in QCD are all equal, and the bare gluon mass is zero. Without gauge invariance, each of these couplings must be tuned independently and a gluon mass introduced to recover QCD. Tuning many parameters in a numerical simulation is very expensive. Continuous symmetries like Lorentz invariance can be given up with less cost because the remaining discrete symmetries of the lattice, though far less restrictive, are still sufficient to prevent the introduction of new interactions with new couplings (at least to lowest order in a).

In contrast to QED, the pure gauge sector of QCD describes a highly non-trivial interacting theory. The self couplings of the gauge potentials are

believed to be responsible for quark confinement. This is the reason why the studies of the pure gauge sector of QCD are of great interest. Furthermore, path integrals involving Grassmann variables are difficult to handle. There are some phenomenological facts in low energy hadron physics like the OZI rule [30] or the approximate linearity of Regge trajectories [31] which suggest that closed quark loops have only a small effect. Most of the numerical QCD calculations have been performed in the pure gauge sector or in the so-called quenched approximation [32, 33] where the effects of pair production processes are neglected. The pure gluonic expectation value of an observable is

$$\langle\, O \,\rangle \;=\; \frac{1}{Z} \prod_{\text{links}} \int dU_{x\mu}\; O(U)\; e^{-S_{\mathrm{G}}} \;, \tag{2.56}$$

with the partition function

$$Z = \prod_{\text{links}} \int dU_{x\mu}\; e^{-S_{\mathrm{G}}} \;. \tag{2.57}$$

The integration measure with the following features

$$\begin{aligned} \int dU \;&=\; 1 \\ \int dU\; f(U) \;&=\; \int dU\; f(VU) = \int dU\; f(UV) \;,\;\; V \in SU(3) \end{aligned} \tag{2.58}$$

is called Haar's measure. In contrast to a path integral in the continuum, (2.56) and (2.57) comprise only a finite number of integrals over the gauge group. No gauge fixing is needed for gauge invariant observables. A four-dimensional hyper-cubic lattice with linear dimension N has $4N^4$ links. An integration over the full gauge group SU(3), for example over the eight Euler angles, has to be performed on each link, resulting in $32N^4$ integrals over a compact interval.

2.6 Continuum Limit

Regularization is a mathematical tool to make calculations possible. In a renormalizable theory, the results are independent of the regularization scheme. Thus the dependence of observables on the lattice regularization with the lattice spacing a as a cutoff parameter has to vanish in the continuum limit, and all symmetries like for example euclidean rotational invariance have to be restored. However, this limit is difficult to achieve.

For simplicity, let us consider a pure gluonic theory, where the only non-dimensionless parameter is the lattice constant a. The calculation of observables on the lattice always gives dimensionless numbers. Their physical dimension has to be determined via the lattice constant. So, a prediction for the physical mass has the form

$$m = \frac{1}{a}\ f(g(a)) \ . \tag{2.59}$$

The continuum limit is achieved when we take a to zero, holding physical quantities fixed. Thus, to obtain a finite mass in the continuum limit, for $a \to 0$ also $f(g(a))$ has to properly converge to zero. The bare coupling constant has to be changed in an appropriate way

$$\left\{ \begin{array}{ll} a & \to 0 \\ g(a) & \to g^* \end{array} \right\} \ , \quad \text{with } f(g^*) = 0 \ . \tag{2.60}$$

In this limit the correlation length $\xi \equiv 1/(ma) \to \infty$ corresponding to a second order phase transition in the lattice theory.

At such a critical point, due to strong long range fluctuations the lattice structure is smeared. Violated symmetries like euclidean rotational invariance are restored. However, an increasing number of lattice points has to be used to preserve the physical extent of the lattice for decreasing a, so that the numerical effort increases enormously. Today, computers are already fast enough to reach the scaling region, where for sufficiently small a the ratio of two physical observables O_1 and O_2 does not depend on the lattice constant even though the individual observables still depend on it:

$$\frac{O_1(g(a),a)}{O_2(g(a),a)} \simeq \frac{O_1(g^*,0)}{O_2(g^*,0)} \ . \tag{2.61}$$

The behavior of $g(a)$ near the critical point can be obtained from the renormalization group equation

$$a\frac{d}{da}\ O(g(a),a)\ |_{a\to 0} = 0 \ ,$$

or

$$\Big[a\frac{\partial}{\partial a} + \beta(g)\frac{\partial}{\partial g}\Big]\ O(g(a),a)\ |_{a\to 0} = 0 \ . \tag{2.62}$$

In QCD the critical coupling g^* is zero and the perturbative expansion of the β-function gives

$$\beta(g) = a\frac{dg}{da} = -\beta_0 g^3 - \beta_1 g^5 + \dots \ . \tag{2.63}$$

Integrating this equation yields the physical value of the lattice constant in the asymptotic scaling regime:

$$a(g) = \frac{1}{\Lambda_{\text{Latt}}} \; e^{-\frac{1}{2\beta_0 g^2}} \; (\beta_0 g^2)^{\frac{\beta_1}{2\beta_0^2}} \; \left(1 + \mathcal{O}(g^2)\right) . \tag{2.64}$$

Λ_{Latt} is the cutoff or scale parameter of the theory. One obtains continuum results in the lattice theory if one can observe a scaling of the computed quantities (e.g. masses ma) with the input coupling g according to (2.64). The calculations of this work were not done in the asymptotic scaling regime. For this reason the physical values of observables can be given only approximately in physical units.

Chapter 3

Meson-Meson Interactions on the Lattice

The various models for the nucleon-nucleon interaction – as outlined in the Introduction – often render a decent description of the experimental data and to some extent give interesting ideas for the underlying interaction mechanism. Nevertheless, their theoretical foundations are inadequate for a fundamental understanding of hadron dynamics. Within the meson exchange models, like Bonn and Paris potentials, the basic QCD degrees of freedom, quarks and gluons, are not taken into account. On the other hand, the bag and quark potential models use artificially introduced boundary conditions or confinement potentials to ensure quark confinement. All these models have various parameters and are ultimately based on phenomenology. For the case of meson-meson interactions the situation is worse. The related experimental information is very poor and therefore less phenomenological models have been developed. One of the aims of modern theoretical nuclear and elementary particle physics is to describe hadron-hadron interactions from first principles. The most promising framework for such investigations is lattice QCD, not least because of the steadily increasing computer power.

Remarkably, only few attempts have been made to extract potentials between two composite hadrons from the lattice [19–22]. Earlier calculations of nucleon-nucleon forces with static quarks have demonstrated that the potential between two three-quark clusters is attractive [21]. A hard repulsive core of the potential, as suggested by experiments and their interpretation, could not be observed in the region where the two nucleons have relative distance close to zero.

In the following a method to obtain interaction potentials in QCD is developed. In particular, the interaction between two heavy-light mesons is investigated. The role of the heavy quarks is to localize the mesons so that their relative distance $\vec{r}$ becomes well defined. The computation of the potential is then based on two-meson time-correlation matrices. Since this method employs dynamics, using quark propagators, in addition to the static heavy-quark gluon-exchange interaction, the calculation will include the effects of interactions between gluons and light quarks, as well as light-quark exchange. Some simulations will also include the effects of sea quarks.

3.1 Quark Propagators

The expectation value of products of quark fields can be expressed in terms of two-point correlation functions of the type

$$\begin{aligned} \langle \psi^a_\alpha(x)\bar{\psi}^b_\beta(x')\rangle_{\rm F} &= \frac{\int \mathcal{D}[\psi]\ \mathcal{D}[\bar{\psi}]\ \psi^a_\alpha(x)\bar{\psi}^b_\beta(x')\ e^{-\bar{\psi}M\psi}}{\int \mathcal{D}[\bar{\psi}]\ \mathcal{D}[\psi]\ e^{-\bar{\psi}M\psi}} \\ &= (M^{-1}(U))^{ab}_{\alpha\beta}(x,x') = G^{ab}_{\alpha\beta}(x,x')\ . \end{aligned} \tag{3.1}$$

The quark propagators G represent the basic quantities not only in hadron spectroscopy, but also many investigations involving hadron systems.

Most of the computational effort of a calculation involving fermions goes into constructing fermion propagators. That is, one wants to solve

$$M(x,y)G(y,z) = \delta(x-z)\,, \tag{3.2}$$

where $M(x,y)$ is the discretized fermion matrix. Since M non-zero elements in the order of the volume square, this is a problem of sparse matrix inversion. It is usually not possible to construct or store $G(x,y)$ for all x and y since this involves finding on the order of (volume)^2 numbers. Instead, one typically constructs $G(x,y)$ for all x and some selected points y by solving

$$M(x,y)\tilde{G}(y,z) = Y(z)\,, \tag{3.3}$$

that is, $\tilde{G}(y,z)$ is the vector $M^{-1}Y$.

In the following we employ the Kogut-Susskind formalism. The fermion matrix of the Kogut-Susskind Lagrangian is

$$(M_{\rm KS})_{xx'} = \frac{1}{2a}\ \sum_\mu \Gamma_{x\mu}[\delta_{x+\hat{\mu},x'}\ U_{x\mu} - \delta_{x,x'+\hat{\mu}}\ U^\dagger_{x'\mu}] + m\ \delta_{xx'}\ . \tag{3.4}$$

The $\Gamma_{x\mu}$ are phases playing the role of the Dirac matrices in the Kogut-Susskind discretization (see Section 2.4.3). The size of this matrix is $(3 \times N_s^3 \times N_t)^2$, where N_s and N_t are the numbers of lattice points in space and in time direction, and the factor 3 are the color degrees of freedom. Even for a very small lattice like $N_s^3 \times N_t = 4^3 \times 8$ $M_{\rm KS}$ becomes a rather big matrix of dimension (1536×1536). Due to the large memory and CPU time requirements instead of a direct numerical inversion of $M_{\rm KS}$ one relies on stochastic methods.

3.1.1 Random Source Technique

This method for inversion of large matrices employs complex vectors with random number components. Usually in studies of time evolution of quark systems we need quark propagators of the type $G(t, t_0)$. They can be obtained by using in (3.3) sources which are non-zero only on one time slice t_0

$$Y_{i,a}(\vec{x}, x_4) = R_{i,a}^{(t_0)}(\vec{x}\,)\delta_{x_4,t_0} \ , \tag{3.5}$$

where R is a complex random vector defined in color and coordinate space with $3L^3$ random number components (random sources) [34, 35]. For an average over N_R random sources one has within statistical errors

$$\frac{1}{N_R}\sum_{i=1}^{N_R} R_{i,a}^{*}(\vec{x}\,)R_{i,b}(\vec{y}\,) = \delta_{\vec{x},\vec{y}}\,\delta_{a,b} \ . \tag{3.6}$$

Solving

$$\sum_{\vec{y}y_4}\sum_{b}(G^{-1})^{ab}(\vec{x}, x_4; \vec{y}, y_4)I_{i,b}^{(t_0)}(\vec{y}, y_4) = R_{i,a}^{(t_0)}(\vec{x}\,)\,\delta_{x_4,t_0} \tag{3.7}$$

for all vectors R_i of the ensemble $(i = 1, \ldots, N_R)$ gives a solution vector I_i for each source R_i

$$I_{i,a}^{(t_0)}(\vec{x}, x_4) = \sum_{\vec{y}b} G^{ab}(\vec{x}, x_4; \vec{y}, t_0)R_{i,b}^{(t_0)}(\vec{y}\,) \ . \tag{3.8}$$

With equation (3.6) single matrix elements of the propagator can be estimated

$$G^{ab}(\vec{y}, t; \vec{x}, t_0) = (M^{-1})^{ab}(\vec{y}, t; \vec{x}, t_0) = \frac{1}{N_R}\sum_{i=1}^{N_R} I_{i,a}^{(t_0)}(\vec{y}, t)R_{i,b}^{*(t_0)}(\vec{x}\,) \ . \tag{3.9}$$

Equation (3.7) must be solved for each gauge field configuration and for each vector R. To keep the CPU times for the calculation of the quark propagator reasonably small, one has to use an effective algorithm for its solution. Since the matrix $M = G^{-1}$ is very large and sparse an iterative method to find a solution is a good choice. When choosing such a method, a matrix inversion problem has to be taken into account. The largest eigenvalue is on the order of m. For small m this means that M is ill conditioned: the ratio of its largest to smallest eigenvalue diverges as $m \to 0$. In practice, the more ill-conditioned the matrix, the harder it is to invert. This is why one generally does not work at the physical value of the quark mass. Instead, one is restricted to unphysically heavy values of the quark mass.

There have been a number of diagnostic studies of matrix inversion algorithms [36]. At present it seems that the most robust algorithm, with the best behavior for small quark mass, is the conjugate gradient algorithm [37].

3.1.2 Hopping Parameter Expansion

The quark propagator G can also be computed within the so-called hopping parameter expansion. Let us write the fermionic action (2.52) in the form

$$S_{\mathrm{F}} = m \sum_{x,y} \bar{\chi}_x K_{xy}[U] \chi_y \,, \tag{3.10}$$

where $K_{xy}[U]$ are matrices in color space:

$$K_{xy}[U] = \delta_{xy} 1 - \frac{1}{2m} M_{xy} \,. \tag{3.11}$$

The only non-vanishing matrices M_{xy} are those connecting neighboring lattice sites:

$$\begin{aligned} M_{x\, x+\hat{\mu}} &= -\Gamma_{x\mu} U_{x\mu} \\ M_{x\, x-\hat{\mu}} &= \Gamma_{x\mu} U^{\dagger}_{x-\hat{\mu},\mu} \,. \end{aligned} \tag{3.12}$$

The inverse of K is the fermion propagator for a given link-variable configuration. For large bare quark mass m we can expand K^{-1} in powers of the hopping parameter $1/2m$ in a Neumann series:

$$K^{-1}[U] = \left(1 - \frac{1}{2m} M\right)^{-1} = \sum_{l=0}^{\infty} \left(\frac{1}{2m}\right)^{\ell} M^{\ell}, \tag{3.13}$$

where M^ℓ is a product of ℓ matrices M_{xy} connecting neighbouring lattice sites, which are given in (3.12). The corresponding expression for the matrix elements of K^{-1} reads:

$$\begin{aligned} K^{-1}_{xa,yb}[U] &= \delta_{xy}\delta_{ab} + \frac{1}{2m}(M_{xy})_{ab} \\ &+ \sum_{l=2}^{\infty}\left(\frac{1}{2m}\right)^{\ell}\sum_{x_i}(M_{xx_1}M_{x_1x_2}\cdots M_{x_{\ell-1}y})_{ab}\,. \end{aligned} \tag{3.14}$$

Using the fact that M_{xy} connects only nearest neighbors on the lattice, the contributions to $K^{-1}_{xa,yb}[U]$ of order $(1/2m)^\ell$ can be computed according to the following rules:

i) Consider all possible paths of length ℓ on the lattice starting at the lattice site x and terminating at the site y.

ii) Associate with each link base at x and pointing in the $\pm\mu$ direction the matrices (3.12).

iii) For each path, take the ordered product of all these matrices following the arrow pointing from x to y, and take the ab-matrix element of this expression.

iv) Sum over all possible paths leading from x to y.

It is easy to see that the matrices M in (3.12) have the following symmetry property:

$$M_{yb,xa} = -M^*_{xa,yb}\ . \tag{3.15}$$

We can obtain a relation between the quark propagator and the antiquark propagator by taking the hermitian conjugate of (3.14), and making use of (3.15):

$$G(y,x) = (-1)^{\sum_\mu (x_\mu + y_\mu)}G^\dagger(x,y)\,. \tag{3.16}$$

Here the "dagger" refers to color indices only. This symmetry is related to CPT invariance, and is the staggered analog of the relation

$$G(y,x) = \gamma_5 G^\dagger(x,y)\gamma_5, \tag{3.17}$$

for the Wilson (naive) fermions. These equations are very useful since if we compute e.g. the propagators of the type $G(t,t_0)$ using the algorithms presented in the previous sections, an extra evaluation of the propagators of the type $G(t_0,t)$ is not necessary.

3.2 Field Operators and Correlation Functions

Since the nucleon-nucleon system containing six light quarks is beyond the current limits of computation, in this section the correlators containing the dynamics of two mesons are derived. In principle the method can be directly extended for the case of baryons. The propagators for the two-meson system were initially derived within a QED_{2+1} model [38–42], the investigations were extended later to QCD_{3+1} [43–47].

The computation of hadron propagators in Kogut-Susskind formalism bears a few technical complications related to the assignment of flavor, space and spin indices [48–50]. In this formalism the quark operators are nonlocal operators which live on elementary hypercubes of the lattice. Thus a meson interpolating field can be defined as

$$\phi_{AB}(x) = \bar{q}(x)(\Gamma_A \otimes \Gamma_B^*)q(x) \tag{3.18}$$

where Γ_A and Γ_B are two of the 16 matrices $\Gamma_b = \gamma_1^{b_1} \dots \gamma_4^{b_4}$ and b labels the location in the hypercube ($b_i = 0$ or 1). By convention, Γ_A acts on spin indices and Γ_B acts on flavor indices. If $\Gamma_A = \Gamma_B$ then the operator $\phi_A \equiv \phi_{AA}$ is local. Otherwise it involves combinations of field operators at different locations in the fundamental hypercube. One must either gauge fix before measurement or explicitly include link factors connecting the sites.

If the operator is local then

$$\phi_A(x) = \sum_b \epsilon_{Ab} \bar{\chi}_b(x) \chi_b(x) \tag{3.19}$$

and ϵ is 1 or –1 depending on whether Γ_B and Γ_A commute or anticommute. In practice this means that a local channel tends to have two particles of opposite parity. This is a characteristic of the Kogut-Susskind formalism causing a special behavior of the correlators. There are four possibilities for local operators: they are (a) $\Gamma = \gamma_5$, $\epsilon_b = (-1)^x$ (pseudoscalar) (b) $\Gamma = 1$ and $\gamma_0\gamma_5$, $\epsilon_b = 1$ (scalar and pseudoscalar) (c) $\Gamma = \gamma_3$ and $\gamma_2\gamma_1$, $\epsilon_b = (-1)^{b_3}$ (vector and tensor) (d) $\Gamma = \gamma_0\gamma_3$ and $\gamma_5\gamma_1$, $\epsilon_b = (-1)^{b_1+b_2}$ (vector and axial vector). Thus a pseudoscalar meson field with momentum $\vec{p} = \frac{2\pi}{L}(k_1, k_2, k_3)$ has the form:

$$\phi_{\vec{p}}(t) = \frac{1}{V} \sum_{\vec{x}} (-1)^{x_1+x_2+x_3+t} e^{i\vec{p}\cdot\vec{x}} \bar{\chi}_f(\vec{x}t) \chi_{f'}(\vec{x}t)\,, \tag{3.20}$$

where f and f' are now the flavors of the Grassmann fields and $V = 3 \cdot N_x \cdot N_y \cdot N_z$. Meson-meson fields Φ with total momentum $\vec{P} = 0$ and spatial

separation $\vec{r}$ then can be defined as

$$\Phi_{\vec{r}}(t) = \sum_{\vec{p}} e^{-i\vec{p}\cdot\vec{r}} \phi_{-\vec{p}}(t)\phi_{\vec{p}}(t). \tag{3.21}$$

Correlations of these field operators contain information about the dynamics of the two-quark and four-quark systems and, ultimately, the effective residual meson-meson interaction.

The two-point correlator, describing the propagation of *one* meson on the lattice is

$$C^{(2)}(t,t_0) = [\langle \phi^\dagger_{\vec{p}}(t)\phi_{\vec{p}}(t_0)\rangle - \langle \phi^\dagger_{\vec{p}}(t)\rangle\langle \phi_{\vec{p}}(t_0)\rangle]_{\vec{p}=0}. \tag{3.22}$$

The four-point time correlation matrix describes the propagation of *two* interacting mesons on the lattice:

$$C^{(4)}_{\vec{r}\vec{s}}(t,t_0) = \langle \Phi^\dagger_{\vec{r}}(t)\Phi_{\vec{s}}(t_0)\rangle - \langle \Phi^\dagger_{\vec{r}}(t)\rangle\langle \Phi_{\vec{s}}(t_0)\rangle. \tag{3.23}$$

Here $\vec{r}$ and $\vec{s}$ are *relative* separations of the meson-meson system. The expressions in (3.22) and (3.23) can be worked out in terms of contractions between the Grassmann fields

$$\ldots \overset{n}{\chi}_f(x)\ldots \overset{n}{\bar{\chi}}_{f'}(x')\ldots = \delta_{ff'}\overset{n}{G}_{xx'}, \tag{3.24}$$

where n indicates the partners of contraction and (G) is the quark propagator. We obtain:

$$\begin{aligned} C^{(2)}(t,t_0) &= \frac{1}{V^2}\langle \sum_{\vec{x},\vec{y}} \mathrm{Tr}(G^\dagger_{\vec{y}t,\vec{x}t_0} G_{\vec{y}t,\vec{x}t_0})\rangle \\ &= \frac{1}{V^2}\langle \sum_{\vec{x},\vec{y}}\sum_{a,b} |G^{ab}_{\vec{y}t,\vec{x}t_0}|^2\rangle \end{aligned} \tag{3.25}$$

$$\begin{aligned} C^{(4)}_{\vec{r}\vec{s}}(t,t_0) &= C^{(4A)} + C^{(4B)} - C^{(4C)} - C^{(4D)} \\ &= \quad + \quad - \quad - \quad , \end{aligned} \tag{3.26}$$

where

$$\begin{aligned} C^{(4A)}_{\vec{r}\vec{s}}(t,t_0) &= \Big\langle \frac{1}{V^2}\sum_{\vec{x},\vec{y}} \mathrm{Tr}(G_{\vec{x}+\vec{r}t,\vec{y}t_0} G^\dagger_{\vec{x}+\vec{r}t,\vec{y}t_0}) \\ &\times \mathrm{Tr}(G_{\vec{x}t,\vec{y}-\vec{s}t_0} G^\dagger_{\vec{x}t,\vec{y}-\vec{s}t_0})\Big\rangle \end{aligned} \tag{3.27}$$

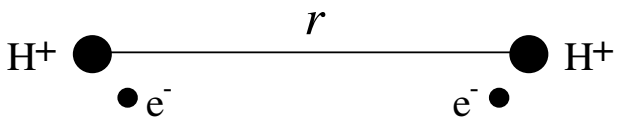

Figure 3.1: The H_2 molecule as a system of two static (heavy) nuclei at relative distance r and two dynamic (light) electrons.

$$
\begin{aligned}
C^{(4B)}_{\vec{r}\vec{s}}(t,t_0) &= \Big\langle \frac{1}{V^2}\sum_{\vec{x},\vec{y}} \mathrm{Tr}(G_{\vec{x}+\vec{r}t,\vec{y}t_0} G^{\dagger}_{\vec{x}+\vec{r}t,\vec{y}t_0}) \\
&\times \mathrm{Tr}(G_{\vec{x}t,\vec{y}+\vec{s}t_0} G^{\dagger}_{\vec{x}t,\vec{y}+\vec{s}t_0})\Big\rangle \qquad (3.28)\\
C^{(4C)}_{\vec{r}\vec{s}}(t,t_0) &= \Big\langle \frac{1}{V^2}\sum_{\vec{x},\vec{y}} \mathrm{Tr}(G^{\dagger}_{\vec{x}+\vec{r}t,\vec{y}t_0} G_{\vec{x}+\vec{r}t,\vec{y}-\vec{s}t_0} \\
&\times G^{\dagger}_{\vec{x}t,\vec{y}-\vec{s}t_0} G_{\vec{x}t,\vec{y}t_0})\Big\rangle \qquad (3.29)\\
C^{(4D)}_{\vec{r}\vec{s}}(t,t_0) &= \Big\langle \frac{1}{V^2}\sum_{\vec{x},\vec{y}} \mathrm{Tr}(G_{\vec{x}+\vec{r}t,\vec{y}t_0} G^{\dagger}_{\vec{x}t,\vec{y}t_0} \\
&\times G_{\vec{x}t,\vec{y}-\vec{s}t_0} G^{\dagger}_{\vec{x}+\vec{r}t,\vec{y}-\vec{s}t_0})\Big\rangle \ . \qquad (3.30)
\end{aligned}
$$

The brackets $\langle \ldots \rangle$ denote the gauge field configuration average, and "trace" and "dagger" operate in color space. The last row of eq. (3.26) contains the schematic representations of different contributions to the correlator $C^{(4)}$. Each of the four contributions comprises the exchange of gluons and sea quarks. For diagrams $C^{(4A)}$ and $C^{(4B)}$ those take place between the mesons, whereas diagrams $C^{(4C)}$ and $C^{(4D)}$ correspond also to interaction mediated by the exchange of valence quarks [51].

3.3 Heavy-Light Meson-Meson System (MM)

The fundamental problem of molecular physics is the explanation of binding of hydrogen atoms in H_2 molecule. This was solved by the help of the adiabatic approximation in which the two light electrons move fast in the electric field of the slowly moving (heavy) protons (Fig. 3.1). The interaction potential of the two atoms was obtained as a function of the distance r of the two protons, which can be considered as the distance of the two atoms. The effective potential of the two atoms was then used to determine the wave functions and energy levels of the H_2 molecule.

Here an analogous problem is considered—a "hadronic molecule" consisting of two heavy-light mesons, in which the heavy quarks are treated as static colour sources, playing the role of the (slow) atomic nuclei. The gluons and light quarks play the role of the fast degrees of freedom. In addition to the static heavy-quark gluon-exchange interaction, this calculation will include the effects of interactions between gluons and light quarks, as well as light-quark exchange. Some simulations will also include the effects of sea quarks.

By making one constituent quark degree of freedom of the meson very heavy one also reduces the complexity of the formulae (3.27)–(3.30) and the heavy-light meson-meson system becomes less costly to simulate. This system contains only two light valence quarks. As such, one is still quite far from a direct simulation of the nucleon problem. However, as all nuclei are hadronic molecules, the qualitative conclusions obtained for this case should be somewhat universal. The resulting interaction potentials are of further interest because they might be used for quantum-mechanical investigations of the two-meson states in a search for exotic particles which are stable against strong decay.

3.3.1 Correlation Functions

The correlators describing the resulting heavy-light mesons, as well as the system of two such mesons (MM) can be obtained from (3.25)–(3.30) by replacing e.g. each quark propagator with the corresponding heavy quark propagator, which can be taken from the hopping-parameter expansion (3.14). We only use the lowest order of the expansion so that the heavy quarks represent fixed color sources. Thus e.g. the heavy-antiquark propagator is given by

$$G^{(h)}_{\vec{x}t_0,\vec{x}t} = \left(\frac{1}{2m_h a}\right)^k [\Gamma_{\vec{x}4}]^k \prod_{j=1}^{k} U_{x=(\vec{x},ja),\mu=4}\,, \tag{3.31}$$

with a similar expression for the quark propagator. The heavy quark mass m_h only gives rise to an irrelevant multiplicative factor in the static approximation and is set to $m_h a = .5$. The phase factors $\Gamma_{\vec{x}4} = (-1)^{(x_1+x_2+x_3)/a}$ in the Kogut–Susskind formulation are remnants of the Dirac matrices and $k = (t - t_0)/a$. Since $G^{(h)}_{\vec{y}t,\vec{x}t_0} \equiv 0$ for $\vec{x} \neq \vec{y}$, all off-diagonal elements of the correlation matrix (3.26) vanish, and we obtain:

$$C^{(2)\mathrm{MM}}(t,t_0) \;=\; \langle \frac{1}{V^2} \sum_{\vec{x}} \mathrm{Tr}(G^{\dagger}_{\vec{x}t,\vec{x}t_0} G^{(h)}_{\vec{x}t,\vec{x}t_0}) \rangle \tag{3.32}$$

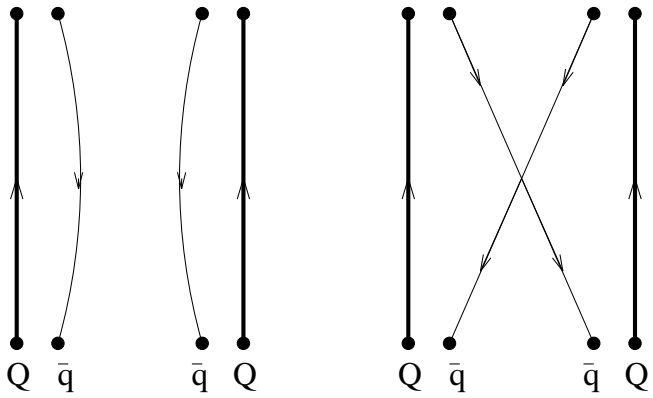

Figure 3.2: (a) Direct term $C^{(4\mathcal{A})}$ and (b) exchange term $C^{(4\mathcal{C})}$ for the MM-system constructed from heavy (Q) and light (q) quark propagators.

$$\begin{aligned} C^{(4)\mathrm{MM}}_{\vec{r}}(t,t_0) &= \langle \frac{1}{V^2}\sum_{\vec{x}} \mathrm{Tr}(G^{(h)}_{\vec{x}+\vec{r}t,\vec{x}+\vec{r}t_0} G^{\dagger}_{\vec{x}+\vec{r}t,\vec{x}+\vec{r}t_0}) \\ &\times \mathrm{Tr}(G^{(h)}_{\vec{x}t,\vec{x}t_0} G^{\dagger}_{\vec{x}t,\vec{x}t_0})\rangle \\ &- \langle \frac{1}{V^2}\sum_{\vec{x}} \mathrm{Tr}(G^{(h)}_{\vec{x}+\vec{r}t,\vec{x}+\vec{r}t_0} G^{\dagger}_{\vec{x}t,\vec{x}+\vec{r}t_0} \\ &\times G^{(h)}_{\vec{x}t,\vec{x}t_0} G^{\dagger}_{\vec{x}+\vec{r}t,\vec{x}t_0})\rangle = C^{(4\mathcal{A})} - C^{(4\mathcal{C})}\,. \end{aligned} \tag{3.33}$$

In the following we omit the superscripts MM. Note that in this case the number of independent contributions to the four-point correlator reduces to two. The diagrams contributing to (3.33) are shown in Fig. 3.2. Figure 3.2(a) corresponds to the pure gluon exchange part while Fig. 3.2(b) corresponds to the flavor exchange part of the mesonic interactions.

The mass m of one heavy-light meson can be extracted from the behavior of the two-point correlator in large euclidean time:

$$C^{(2)}(t,t_0) \propto e^{-m(t-t_0)}. \tag{3.34}$$

The state with minimal energy of the meson-meson system can be extracted from the large euclidean time behavior of the four-point correlator following quantum-mechanical reasoning [17,52]. Similar arguments for composite particles were presented in [41, 44]. In the euclidean formulation of quantum mechanics the spectral decomposition of the four-point Green function

representing the two-meson system is

$$C^{(4)}_{\vec{r}\vec{s}}(t,t_0) = \sum_n \langle \Phi^\dagger_{\vec{r}}|n\rangle\langle n|\Phi_{\vec{s}}\rangle e^{-E_n(t-t_0)}\,, \tag{3.35}$$

where E_n are the energy eigenvalues and $|n\rangle$ are the associated eigenstates. For a given potential we can solve the energy eigenvalue problem to obtain E_n and $|n\rangle$ and calculate the sum in (3.35). We invert this process and calculate the potential from a given Green function. As the heavy quarks lead to a localization of the mesons during the time evolution of the system, we have $|\vec{r}| = |\vec{s}| = r$ giving

$$C^{(4)}_r(t,t_0) = \sum_n |\langle \Phi^\dagger_r|n\rangle|^2 e^{-E_n(t-t_0)}. \tag{3.36}$$

Since the correlation matrix $C^{(4)}$ describes the time evolution of the meson-meson system with a constant particle separation r for the whole process, we can extract the energy of two heavy-light mesons from the asymptotic time behavior at fixed r [17, 41, 44, 52]

$$C^{(4)}_r(t,t_0) \propto c_4(r) e^{-W(r)(t-t_0)}. \tag{3.37}$$

The effective interaction potential is obtained by subtracting from $W(r)$ the total energy $2m$ of the non-interacting two-meson system:

$$V(r) = W(r) - 2m\,. \tag{3.38}$$

3.3.2 Autocorrelation of the Two-Point Function

Before engaging in costly lattice simulations, one has to fix the simulation parameters to avoid systematic errors. One source of error is the autocorrelation of the correlation functions.

Statistically independent gauge field configurations can be generated via a Markov chain. To get an idea after how many successive Markov steps one can expect independent results for an operator O one may calculate the autocorrelation function

$$A(\tau) = \frac{\frac{1}{N_I-\tau}\Big[\sum_{i=1}^{N_I-\tau} O(i+\tau)O(i) - \frac{1}{N_I-\tau}\sum_{i=1}^{N_I-\tau} O(i+\tau)\ \sum_{i=1}^{N_I-\tau} O(i)\Big]}{\frac{1}{N_I}\Big[\sum_{i=1}^{N_I} O^2(i) - \frac{1}{N_I}\big(\sum_{i=1}^{N_I} O(i)\big)^2\Big]}\,. \tag{3.39}$$

For this purpose the operator O has to be evaluated on N_I successive gauge field configurations. Theoretically $A(\tau)$ is an exponentially decreasing curve

in the limit $\tau \to \infty$. After τ_0 iterations the function A is close enough to zero to expect independent results for O when performing τ_0 sweeps between two measurements. In Figure 3.3 we plot $A(\tau)$ for $O = C^{(2)}(t_0, t_0)$ (a), and for $O = C^{(2)}(t_p, t_0)$ (b) for various time extents $N_t = 8, 16, 32$ of a $4^3 \times N_t$ lattice. With our choice of the random sources we fixed $t_0 = 0$. The minimum of the correlation function on a periodic lattice is at $t_p = N_t/2$. The inverse gluon coupling is $\beta = 5.2$. Sea quarks with mass $m_q a = 0.1$ and $n_f = 3$ flavors are included in the simulation. The mass of the valence quarks is also $m_f a = 0.1$. From Figure 3.3 it can be seen that for $\tau > 150$ independent results for the meson two-point function can be expected.

3.3.3 Number of Random Sources

In this section we try to find out how many random sources have to be employed to obtain reliable results for the correlators. For this purpose the two-point correlator of a heavy-light meson (3.32) is calculated in a quenched simulation on a $8^3 \times 16$ lattice for $\beta = 5.6$ and $m_f a = 0.1$. In Fig. 3.4 the meson correlator is plotted against the number of random sources on a double logarithmic scale. The largest ensemble consisted of $N_R^{\max} = 128$ random sources. The results from a single gauge field configuration are compared with the averages over twenty gauge fields for $t = 0, 1$ and 2. In both cases the correlator converges reasonably well above $N_R = 16$. The behavior of the correlator becomes worse for larger final times t. As expected, the convergence of the correlator with increasing N_R improves for averages over more gauge fields.

In Fig. 3.5 we show a similar comparison for the two contributions to the heavy-light meson-meson correlator (3.33) from a single gauge field configuration and from an average over twenty gauge field configurations for separation $r = 0$. Again the correlators are drawn for $t = 0, 1$ and 2. One can see that $C^{(4\mathcal{A})}$ and $C^{(4\mathcal{C})}$ have larger fluctuations than $C^{(2)}$ especially for one gauge field configuration. But we observe a sufficient convergence for the average over twenty fields already for $N_R \approx 32$ random sources.

3.3.4 MM-Potentials

Quenched results

The gauge field configurations of pure QCD were generated on a periodic $N_s^3 \times N_t = 8^3 \times 16$ lattice with inverse gauge coupling $\beta = 5.6$. According to the renormalization group equation this corresponds to a lattice spacing

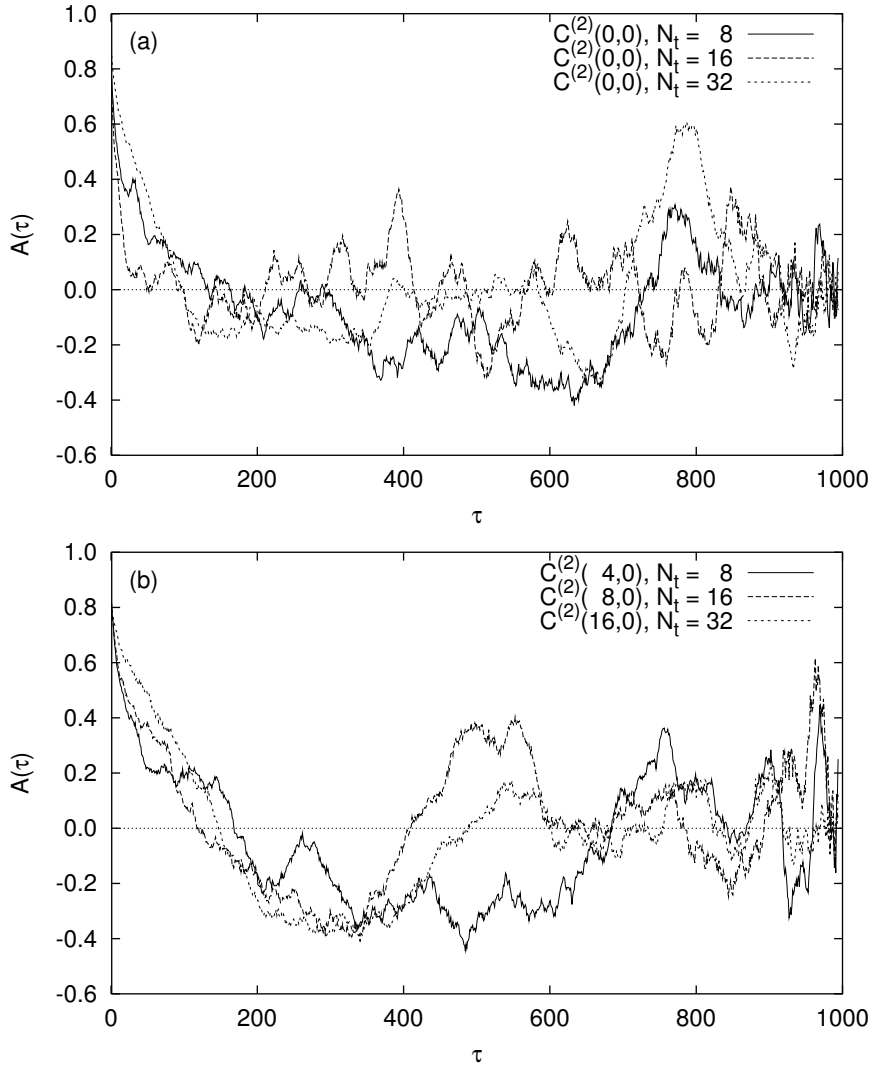

Figure 3.3: Autocorrelation $A(\tau)$ (3.39) for the single-meson two-point function $C^{(2)}(t_0, t_0)$ (a) and $C^{(2)}(t_p, t_0)$ (b) corresponding to (3.25) on a $4^3 \times N_t$ lattice for $N_t = 8, 16, 32$.

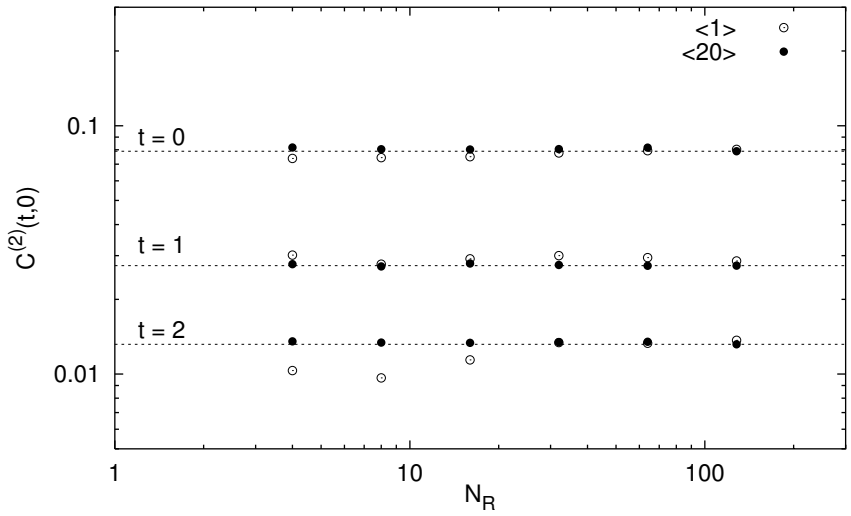

Figure 3.4: Two-point correlation function $C^{(2)}(t, t_0)$ from (3.32) as a function of N_R for $t = 0, 1$ and 2 and $t_0 = 0$. The convergence of the correlator is compared for a single and an average over twenty configurations on a $8^3 \times 16$ lattice for $\beta = 5.6$ and $m_f a = 0.1$.

$a \approx 0.19$ fm. The results were obtained from an analysis of 100 configurations separated by 200 updates of the gauge fields (see Section 3.3.2). For the smallest quark mass 200 configurations were produced to improve statistics. The light-quark propagators with different mass parameters $m_f a$ in the range 0.025–0.2 were determined from the inversion of the fermionic matrix (3.4) using the conjugate gradient algorithm with 32 random sources (see Sections 3.1.1 and 3.3.3). To reduce the computational effort we did not average over different values of t_0 in the inversion process.

The light-quark propagators obtained by the inversion contain contributions both from (anti)quarks winding around the periodic lattice. To improve our statistics we took into account also heavy-quark propagators winding in the opposite direction for separations larger than $N_t/2$. In this way the correlators become symmetric about the center of the time-axis. The contribution in the heavy-quark propagators arising from the longer of the two lines is suppressed in powers of m_h and is ignored.

We calculated the four-point propagator for different values of the meson separation r/a from 0 to 4 averaging over all spatial directions. Non-integer

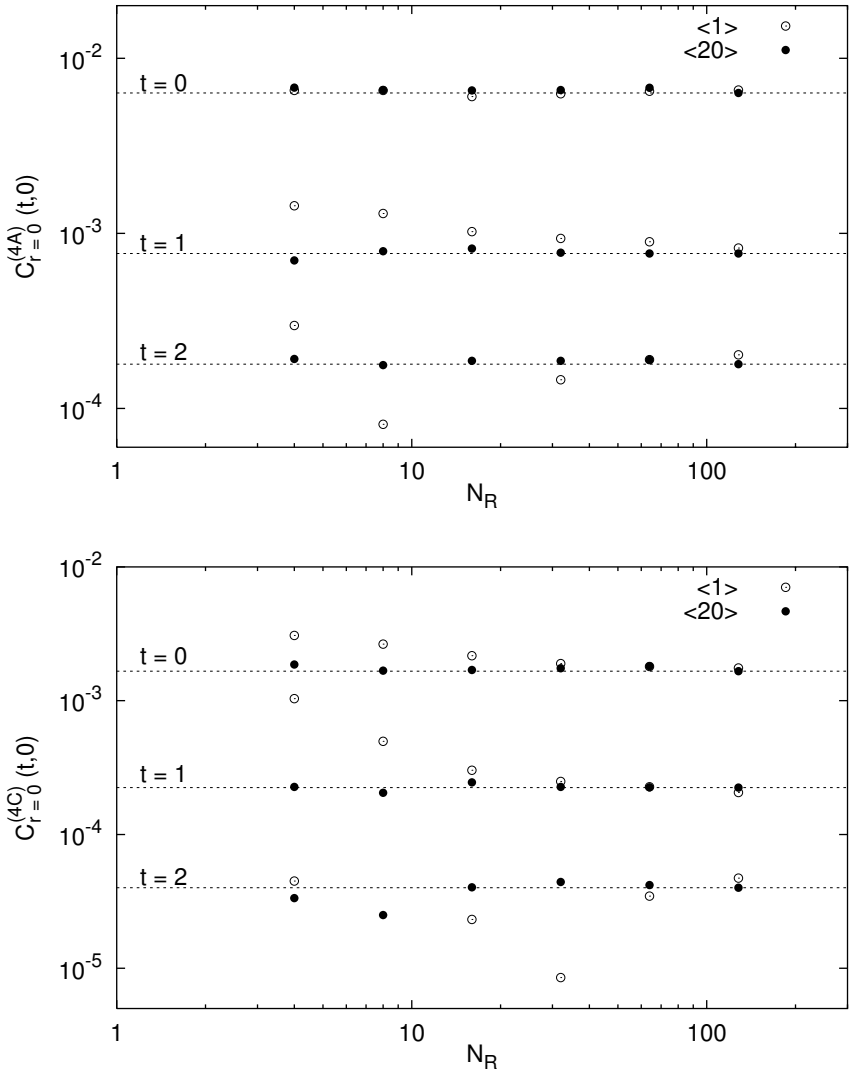

Figure 3.5: Four-point correlators $C^{(4\mathcal{A})}$ and $C^{(4\mathcal{C})}$ of the heavy-light meson-meson system as a function of N_R for $t = 0, 1$ and 2. Comparison of the convergence of the correlators for one and an average over twenty gauge field configurations on a $8^3 \times 16$ lattice for $\beta = 5.6$ and $m_f a = 0.1$.

distances $r/a = \sqrt{2}, \sqrt{3}$, etc. were also included in order to estimate systematic errors on $W(r)$ related to violation of rotational O(3) invariance by the lattice.

The potential was extracted from cosh-fits to the correlators. In the following we set $t_0 = 0$. Because of the periodicity in time one expects the following behavior for $C^{(2)}$ and $C^{(4)}$:

$$\begin{aligned} C^{(2)}(t) &= \sum_n A_n \cosh\left[m_n(t - N_t a/2)\right] \\ &+ (-1)^{t/a} \sum_n \widetilde{A}_n \cosh\left[\widetilde{m}_n(t - N_t a/2)\right] \qquad (3.40) \\ C_r^{(4)}(t) &= \sum_n B_n(r) \cosh\left[W_n(r)(t - N_t a/2)\right] \\ &+ (-1)^{t/a} \sum_n \widetilde{B}_n(r) \cosh\left[\widetilde{W}_n(r)(t - N_t a/2)\right]. \qquad (3.41) \end{aligned}$$

The terms alternating in sign are a peculiarity of the Kogut-Susskind formulation of lattice fermions and correspond to contributions from intermediate states of opposite parity (see discussion of Eq. (3.19)). A precise analysis is needed in order to estimate the number of excited states contributing to the sums in Eqs. (3.40) and (3.41) [53]. We analyzed the correlation functions by using fewer data points corresponding to asymptotic times and looked at the stability of the potentials from the fit. The outcome of this analysis is presented in Fig. 3.6. Unfortunately fewer data points for the fit yield larger error bars in the potential, but especially for $m_f a = 0.2$, when the statistical errors remain reasonably small, one can see that the contribution from excited states does not alter the shape of the potential considerably. The same conclusion could be drawn from a refined analysis on a $10^3 \times 20$ lattice (see later). Thus, we included all points in time direction to extract the lowest contribution from both terms in eqs. (3.40) and (3.41) risking to slightly overestimate the mass parameters. However, it turned out that a four-parameter fit of A_1, m_1, $\widetilde{A}_1$, $\widetilde{m}_1$ and $B_1(r)$, $W_1(r)$, $\widetilde{B}_1(r)$, $\widetilde{W}_1(r)$ gives a satisfactory result with an acceptable χ^2. As an example, in Fig. 3.7 we show the numerical results for the two-point correlator as well as for the four-point correlator at $r = 0$ with $m_f a = 0.1$, and fits to the data points. The Levenberg-Marquardt method described in [54] was employed. The solid curves correspond to the functions in (3.40) with the parameter set A_1, m_1, $\widetilde{A}_1$, $\widetilde{m}_1$ and in (3.41) with $B_1(0)$, $W_1(0)$, $\widetilde{B}_1(0)$, $\widetilde{W}_1(0)$, respectively. Note that one correlation function is represented by two curves distinguishing between even and odd distances. The mass of the meson is identified by

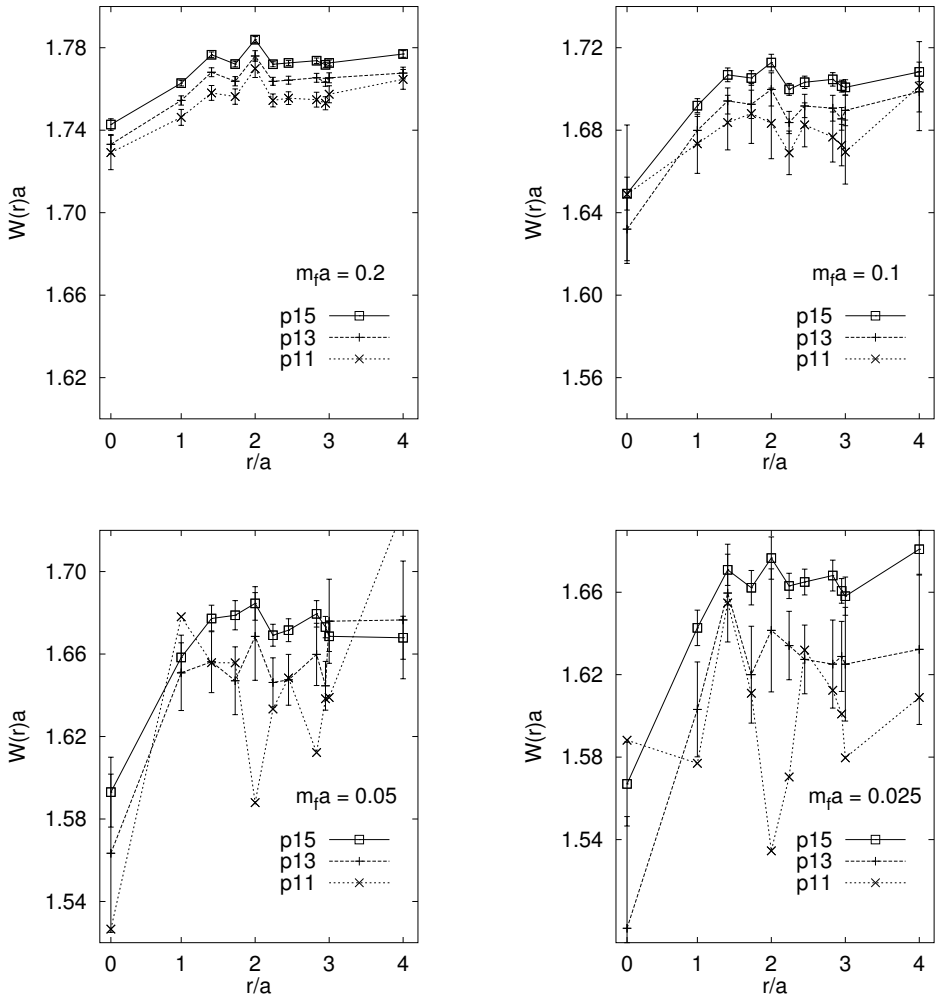

Figure 3.6: Meson-meson energies $W(r)a$ for different light quark masses $m_f a$. Different data sets represent different number of data points corresponding to asymptotic times used for the fit, e.g. p15 = 15 data points. Some error bars are omitted for clarity of the figures. Lines connecting the symbols are to guide the eye.

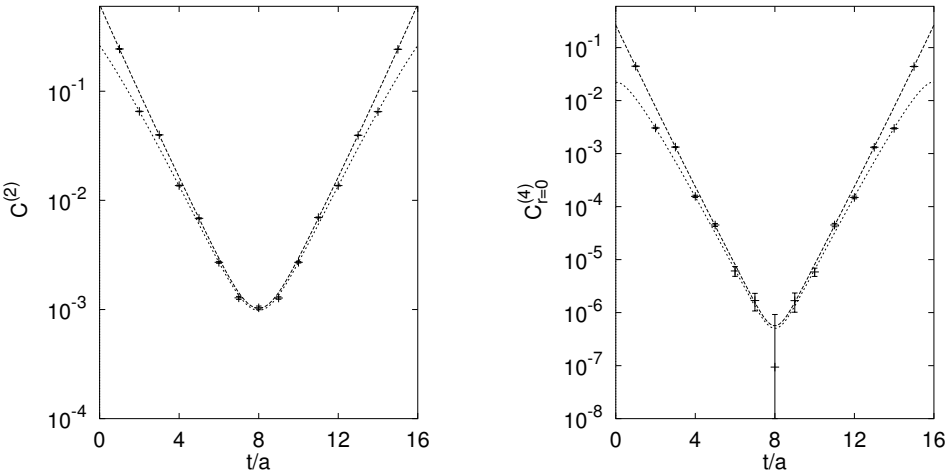

Figure 3.7: Time dependence of the computed correlation functions and fits to $C^{(2)}$ and $C^{(4)}_{r=0}$ with $m_f a = 0.1$ (see text).

$m = m_1$ and the meson-meson energy by $W(r) = W_1(r)$.

A comparison of the direct term $C^{(4\mathcal{A})}$ and the quark-exchange term $C^{(4\mathcal{C})}$ indicates a leading contribution from $C^{(4\mathcal{A})}$ being almost an order of magnitude larger than $C^{(4\mathcal{C})}$. The reason is that due to the strong confining force the possibility for light valence quarks to be exchanged between the mesons is very small.

In Fig. 3.8 we repeat and discuss now the results of $W(r)$ for different light-quark mass parameters from Fig. 3.6. The horizontal lines correspond to the energies $2m$ of two independent mesons. The error bars were obtained by taking into account the statistical errors of the correlators $C^{(2)}$ and $C^{(4)}$ in the fit and estimating the covariance matrix of the standard errors in the fitted parameters (see [54]). For smaller m_f the error bars increase due to the inaccuracy of the inversion of the fermionic matrix. The curves reach their plateau at $r/a \approx 2$, continuing, with large fluctuations, to the asymptotic values $2m$. To be numerically consistent with $W(r)$ at large distances, the mass $2m$ of two non-interacting mesons was extracted from fits to the square of the meson two-point function $[C^{(2)}]^2$. We should point out that interaction energies in Fig. 3.8 are only about 5×10^{-2} of a typical hadron mass. This is characteristic of residual hadronic forces.

The resulting potentials are collected in Fig. 3.9. The error bars are

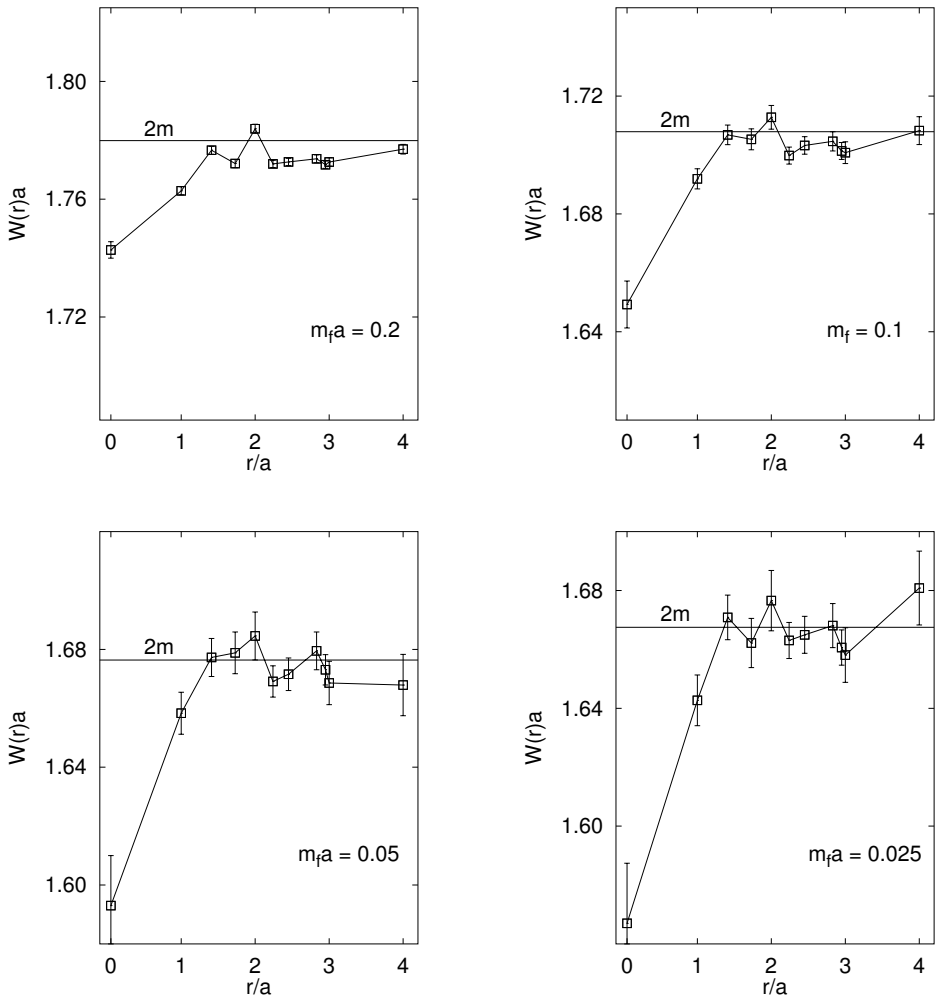

Figure 3.8: Meson-meson energies $W(r)$ for several light-quark masses. Data points at degenerate distance $r/a = 3$ are slightly shifted. The error bars were obtained by taking into account the statistical errors in the fit. Lines connecting the symbols are to guide the eye.

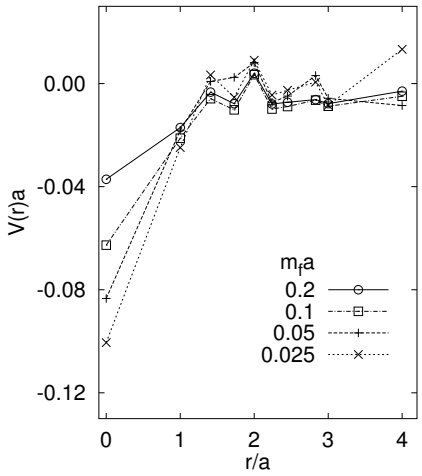

Figure 3.9: Meson-meson potentials $V(r) = W(r) - 2m$ for different light-quark masses m_f. Error bars are omitted and data at $r/a = 3$ are averaged.

omitted and the data at distance $r/a = 3$ are averaged for the sake of clarity of the figure. Attraction for short distances is evident. We find that the interaction is stronger for smaller light-quark masses, but its range is always approximately the same. The reason is that confinement forces suppress the exchange of quarks at large separations. Quark exchange plays a significant role only for distances r much less than $2a$. The systematic deviations in the off-axes directions may originate from anisotropy effects of the cubic lattice. This issue will be studied in Section 3.5.

Simulation with dynamic quarks

The interaction between nucleons is mediated by the exchange of virtual mesons. The quenched approximation used so far in our simulation does not allow for the creation of virtual $q\bar{q}$-pairs, which would ultimately lead to the formation of the mediating mesons, as shown in the first diagram of Fig. 3.10. Remarkably, even in the quenched approximation the exchange term in (3.33) will include pion exchange contributions—one such exchange is shown in the second diagram of Fig. 3.10. Nevertheless, in order to elucidate how significant the contribution of the dynamic quarks to the interaction potential is, a full QCD investigation of the heavy-light meson-meson system was performed. For the inclusion of dynamic fermions the pseudo-fermionic

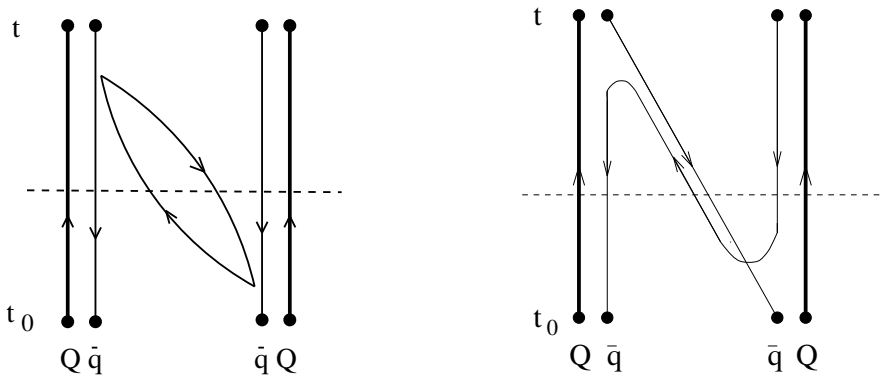

Figure 3.10: Meson-exchange contributions to the meson-meson propagator. At the time slices indicated by the dotted lines, two heavy-light mesons and a light meson are present. Diagram (a) implies the creation of a virtual $q\bar{q}$ pair, whereas (b) is present also in the quenched approximation.

method was used [55]. The number of flavors was set to $n_f = 3$, with the dynamic quark mass $m_q a = 0.1$. The choice of a coupling $\beta = 5.2$ leads to a lattice constant comparable with that of the quenched simulation. The results with and without dynamic quarks for light valence-quark mass parameter $m_f a = 0.1$ are presented in Fig. 3.11. The outcome is the same within statistical errors, and suggests that the influence of the dynamic quarks is not considerable. This turns out at least for our dynamic quark mass which is around $m_q \approx 100\,\mathrm{MeV}$ and reflects a general fact found in lattice QCD computations.

Simulation on a 10^3x 20 lattice

To see how the finite extent of the space-time lattice affects the resulting interaction potentials, here the quenched results presented before are compared with a quenched simulation on a larger, $N_s^3 \times N_t = 10^3 \times 20$ lattice with the same inverse gauge coupling $\beta = 5.6$ and light-quark mass $m_f a = 0.1$. Because of limited computer resources the results for the larger lattice were obtained from an analysis of only 50 configurations separated by 200 updates of the gauge fields.

Recall that the meson mass and the potential were extracted from cosh-fits to the correlators of the form (3.40) and (3.41), respectively, where only the lowest contributions to the sums were considered. Therefore these are

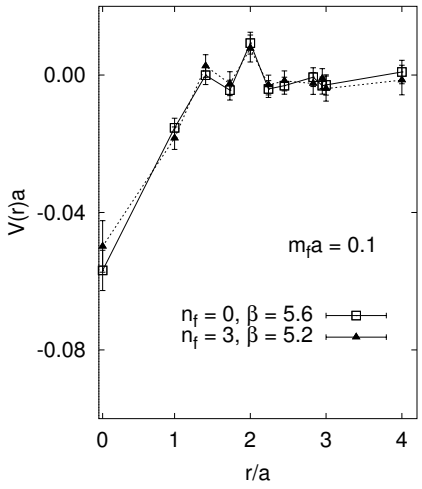

Figure 3.11: Heavy-light meson-meson potentials $V(r)a$ for quark mass $m_f a = 0.1$, comparing a quenched simulation with $\beta = 5.6$ and a full QCD simulation with $\beta = 5.2$ and number of flavors $n_f = 3$.

effective-mass fits, since the contributions of all the excited states are included into one mass parameter. For large times t, however, the contributions of excited states are suppressed, and the effective mass only contains the state with minimal energy. Figure 3.12 shows the effective mass $2m = 2m_1$ of two non-interacting mesons resulting from a fit of (3.40) to the correlator $[C^{(2)}]^2$ as a function of the first time slice t_f of the correlator considered for the four-parameter fit. In other words, $N_{\mathrm{dp}} = N_t + 1 - 2t_f$ data points of the correlator around $N_t a/2$ were taken into account for the fits for a given t_f. The simulations on the $8^3 \times 16$ and $10^3 \times 20$ lattices are compared. In both cases a plateau is reached for increasing t_f. This can be seen more clearly for the larger lattice, where the lowest mass value is obtained already for $t_f = 2$. For the smaller lattice the last stable fit could be obtained for $t_f = 4$, whereas for the larger lattice the fits were stable up to $t_f = 5$. For larger t_f the errors increase reflecting the larger errors of the correlator for asymptotic times.

Figure 3.13 displays the effective total meson-meson energy $W(r) = W_1(r)$ for $r = 0, 1$ and 2, again as a function of the first time slice t_f considered for the four-parameter fit (3.41) for $C_r^{(4)}(t, t_0)$. The results for the smaller and larger lattice behave similarly. It is unclear whether a plateau is

reached because of the large statistical errors for large t_f, but the behavior of the data points for increasing t_f hints at a plateau already at $t_f = 3$. Again, the plateau is approached faster for the larger lattice.

The limited volume of the lattice poses an additional problem. Because of the periodic boundary conditions the interaction energy can also have contributions from the interaction of the meson-meson system with its "mirror" particles. We now consider a fixed hadron that interacts with another hadron separated by some distance r on the original lattice. The interaction of the first hadron with its own mirror particles in the periodic lattices may lead to an additive constant in the potential. If so, changing the spatial extent of the lattice would lead to a change in the resulting interaction potentials. The potentials from the simulations on the two different lattices—with all data points included into the fits of the correlators, $t_f = 1$—are presented in Fig. 3.14. The outcome is the same within statistical errors indicating that a spatial volume of 8^3 is big enough to accommodate the heavy-light meson-meson system. This figure also presents the resulting meson-meson potentials from the simulation on the larger lattice with the first time slice $t_f = 3$ of the correlator considered for the four-parameter fit. Here the contributions from excited states are at least partly eliminated. Comparing with the $t_f = 1$ results one can see that the shape of the potential remains stable. This is a hint that also for lattices with larger time extents, where the extraction of the ground state becomes feasible, the qualitative behavior of the potential may be the same. This result also suggests that the excited states of the four-quark system are not resonant states of the meson-meson system but rather excitations within the individual mesons.

3.3.5 Exotic Mesons as Two-Meson "Molecules"

An exotic meson has a structure which is different from that of a normal meson. A normal meson has the quantum numbers of a possible bound state of a quark and an antiquark: so-called normal quantum numbers. A meson which does not have normal quantum numbers is said to have exotic quantum numbers, and is by definition exotic. Some physicists think that mesons with exotic quantum numbers ought to exist because QCD does not obviously forbid them, but there is not yet definitive experimental evidence for the existence of any such meson.

A meson may have normal quantum numbers and still be exotic if its internal structure differs from that of a normal meson. Although there are candidates for such exotics, none has yet been positively identified. The

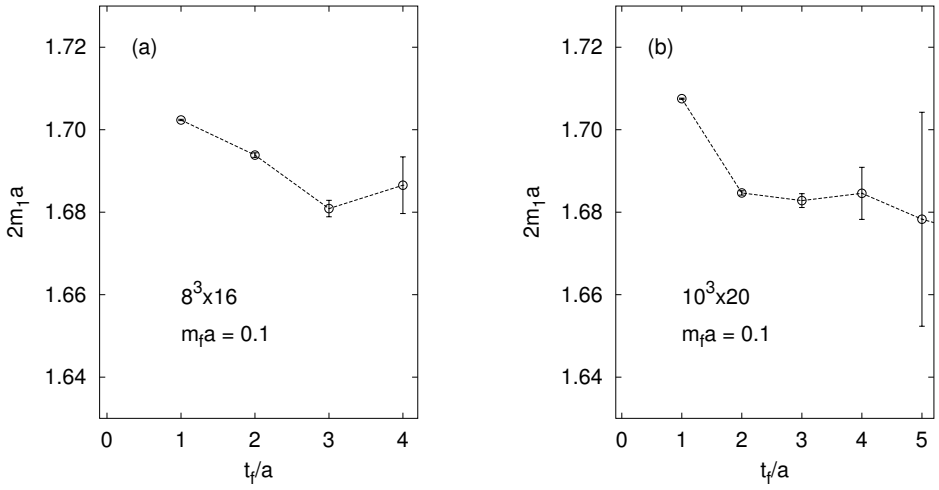

Figure 3.12: Effective mass $2m = 2m_1$ of two non-interacting mesons as a function of the first time slice t_f of the correlator included into a four-parameter fit for light-quark mass $m_f a = 0.1$, comparing simulations on a $8^3 \times 16$ (a) and a $10^3 \times 20$ (b) lattice.

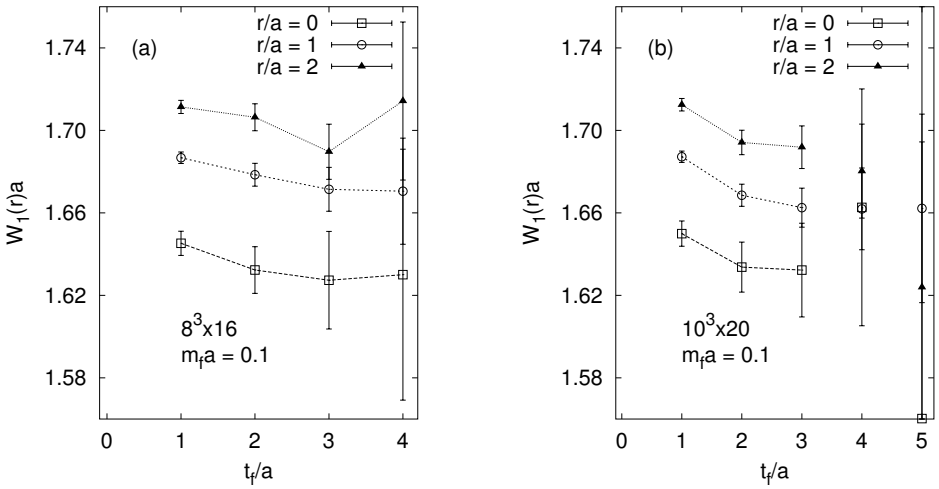

Figure 3.13: Effective meson-meson energy $W(r) = W_1(r)$ for $r = 0, 1, 2$ as a function of the first time slice t_f of the correlator included into the four-parameter fit for quark mass $m_f a = 0.1$, comparing simulations on a $8^3 \times 16$ (a) and a $10^3 \times 20$ (b) lattice.

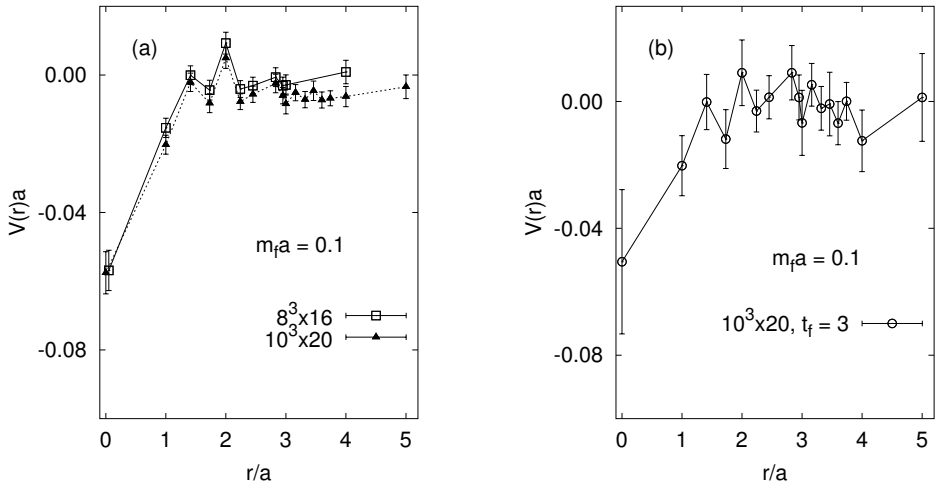

Figure 3.14: (a) Meson-meson potentials $V(r)a$ for quark mass $m_f a = 0.1$, comparing simulations on a $8^3 \times 16$ and a $10^3 \times 20$ lattice, respectively. (b) $V(r)a$ for the larger lattice with the first time slice $t_f = 3$ of the correlator included into the fit.

problem of how to distinguish between a normal and an exotic meson with the same normal quantum numbers is a difficult one and remains unsolved, although progress has been made.

In a model with only constituent quarks and constituent gluons, a normal meson is composed of a quark and antiquark. Among possible exotic mesons there might be glueballs (composed of gluons only), hybrids (composed of a quark, antiquark, and gluons), diquark-antidiquark states and meson "molecules" (composed of two normal mesons). The evidence for the existence of exotic mesons is slowly accumulating, but is not yet definitive [56].

While there is a long history of glueball mass calculations in lattice QCD, including attempts to use lattice calculations to identify experimentally observed mesons with glueballs [57, 58], and there are also some recent lattice computations of hybrid meson masses [59, 60], meson-molecule or diquark models of exotic mesons have not been treated on the lattice. (For a phenomenological diquark model see [61].) Starting from the lattice results presented in the previous section we make a first attempt to examine the possibility of formation of a stable exotic meson molecule composed by two

heavy-light mesons.

First we determine the quantum numbers of our four-quark system. In the isospin representation we have $\phi_{II_3} = \phi_{\frac{1}{2}\pm\frac{1}{2}}$ for the heavy-light meson fields in (3.20) and therefore the two-meson system defined by (3.21) forms an $I = 1$, $I_3 = \pm 1$ state. For the case of two mesons of an isospin doublet, defined by the field

$$\Phi_{\vec{r}}(t) = (\sqrt{2}V)^{-1} \sum_{\vec{x}} \sum_{\vec{y}} \delta_{\vec{r},\vec{y}-\vec{x}} \left[\phi_{\frac{1}{2}+\frac{1}{2}}(\vec{x}t)\phi_{\frac{1}{2}-\frac{1}{2}}(\vec{y}t) + \phi_{\frac{1}{2}-\frac{1}{2}}(\vec{x}t)\phi_{\frac{1}{2}+\frac{1}{2}}(\vec{y}t) \right] , \tag{3.42}$$

one has a $I = 1$, $I_3 = 0$ state. Replacing the field (3.42) into the defining formula of the four-point correlator (3.23) yields again (3.33) in the heavy-light approximation, provided that the light (u and d) quark masses are degenerate. Thus the MM states corresponding to different I_3s are approximately identical. When computing the four-point correlators we sum over all spatial directions, therefore we project into the s-wave part of the correlators, describing a state with $J^P = 0^+$.

Lattice computations are easier for large quark masses (see Section 3.1.1). The light-quark masses used in our simulations are in the range $m_f \approx 25 \div 200\,\mathrm{MeV}$ which is much greater than the mass of a u or d quark. Since neither the full QCD simulation nor the simulation on the larger lattice led to substantial changes of the results, we took the data from the original run (Fig. 3.9) for this investigation. In this way we could make an extrapolation of the data for different quark masses towards the chiral limit, getting closer to the masses of the light physical quarks. By a two-parameter fit to the resulting data points using a Gaussian function we obtained an analytic form for the meson-meson interaction potential which is shown in Figs. 3.15(a). The interaction potential was then used as an input to the Schrödinger equation for a phase shift calculation. The resulting phase shifts are displayed in Fig. 3.15(b) with a variation in the meson mass. The extrapolated meson mass reads $ma = 0.83$.

Although the potential is attractive, the computed phase shifts signal the absence of a bound state. For a decisive check, the meson mass and the interaction potential were used as an input for a resonant state searching program presented in [62]. Neither bound nor resonant meson-meson states were found. This is in agreement with the predictions of most of the phenomenological models. Whether such exotic mesons exists or not has to be answered by future experiments.

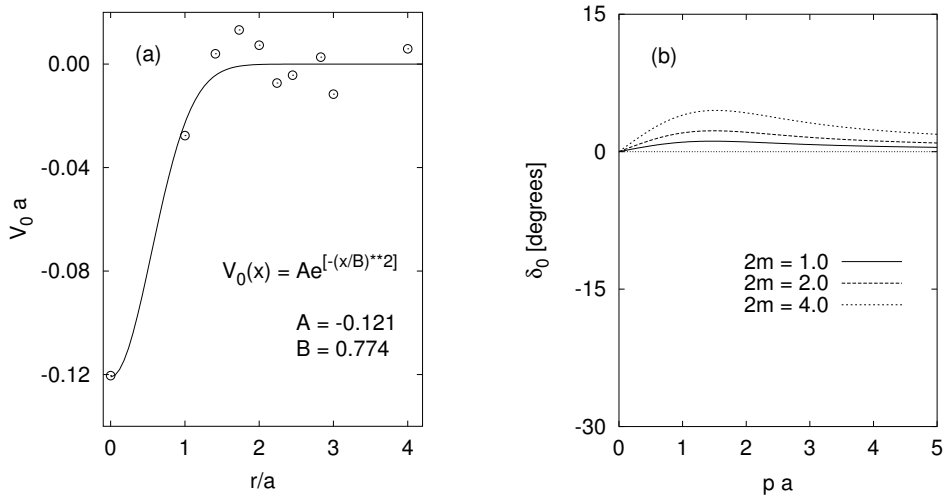

Figure 3.15: Heavy-light meson-meson potentials from the simulation data in Fig. 3.9 extrapolated to the chiral limit (a), together with the resulting phase shifts δ (b).

3.4 Heavy-Light Meson-Antimeson System (M$\bar{\text{M}}$)

In this section we extend our lattice investigations of meson-meson interactions to a system consisting of a heavy-light meson (M) and its antiparticle ($\bar{\text{M}}$). Simulations of M$\bar{\text{M}}$-systems are of great interest because of their immediate application to $K\bar{K}$ phenomena. Studies of multi-quark states indicate that the only likely bound four-quark systems are mesonic molecular states [63]. Two exotic particles, the $a_0(980)$ and $f_0(975)$, are thought to be lightly-bound $K\bar{K}$ molecules [64]. From the production processes of f_0 and a_0 (which both decay into $K\bar{K}$ pairs) scalar-isoscalar $K\bar{K}$ potentials have recently been extracted by inverse scattering theory [65, 66]. This opens up the possibility of an indirect comparison of our lattice QCD results with the experiment.

By deriving suitable correlators for the meson-antimeson system, we compute M$\bar{\text{M}}$ potentials in different isospin channels. The $I = 0$ potential in the $I = 0$ channel is then compared with the $K\bar{K}$ potentials obtained from inverse scattering theory calculations. Searches for M$\bar{\text{M}}$ resonant states are also performed.

3.4.1 Correlation Functions

The correlators describing the $\mathrm{M\bar{M}}$ system in the $I = 1$ channel can be derived in a similar way as for the MM case. The one-antimeson fields corresponding to the one-meson fields defined in (3.20) are:

$$\phi^{\bar{\mathrm{M}}}_{\vec{p}}(t) = \frac{1}{V}\sum_{\vec{x}}(-1)^{x_1+x_2+x_3+t}e^{i\vec{p}\cdot\vec{x}}\bar{\chi}_{f'}(\vec{x}t)\chi_f(\vec{x}t)\,. \tag{3.43}$$

The two-point correlator of an antimeson can be defined as in (3.22). Substituting the fields by $\phi^{\bar{\mathrm{M}}}$ we obtain the complex conjugate of the formula (3.32), which will ultimately yield the same results as the two-point correlator of the heavy-light mesons, reflecting the fact that the mass m of a heavy-light antimeson is identical with that of a meson.

Inserting the meson-antimeson fields

$$\Phi^{\mathrm{M\bar{M}}}_{\vec{r},I=1}(t) = \sum_{\vec{p}} e^{-i\vec{p}\cdot\vec{r}}\phi^{\mathrm{M}}_{-\vec{p}}(t)\phi^{\bar{\mathrm{M}}}_{\vec{p}}(t) \tag{3.44}$$

into the defining formula of the four-point correlator (3.23) and performing the contractions we obtain:

$$\begin{aligned}
C^{(4)\mathrm{M\bar{M}}}_{\vec{r},I=1}(t,t_0) \;=\;& \frac{1}{V^2}\langle\sum_{\vec{x}}\mathrm{Tr}(G^{(h)\dagger}_{\vec{x}+\vec{r}t,\vec{x}+\vec{r}t_0}G_{\vec{x}+\vec{r}t,\vec{x}+\vec{r}t_0})\,\mathrm{Tr}(G^{(h)}_{\vec{x}t,\vec{x}t_0}G^{\dagger}_{\vec{x}t,\vec{x}t_0})\rangle \\
&- \frac{1}{V^2}\langle(-1)^{t+t_0}\sum_{\vec{x}}\mathrm{Tr}(G^{(h)\dagger}_{\vec{x}+\vec{r}t,\vec{x}+\vec{r}t_0}G_{\vec{x}+\vec{r}t,\vec{x}t} \\
&\times G^{(h)}_{\vec{x}t,\vec{x}t_0}G_{\vec{x}t_0,\vec{x}+\vec{r}t_0})\rangle \\
&- \frac{1}{V^2}\langle\sum_{\vec{x},\vec{y}}(-1)^{\sum_\mu(x_\mu+y_\mu)}\,\mathrm{Tr}(G^{\dagger}_{\vec{x}t,\vec{y}t_0}G_{\vec{x}t,\vec{y}t_0})\rangle\delta_{\vec{r},0} \\
&+ \frac{1}{V^2}\langle\sum_{\vec{x},\vec{y}}\mathrm{Tr}(G^{\dagger}_{\vec{y}t_0,\vec{y}t_0})\,\mathrm{Tr}(G_{\vec{x}t,\vec{x}t})\rangle\delta_{\vec{r},0} \\
&- \frac{1}{V^2}\langle\sum_{\vec{y}}\mathrm{Tr}(G^{\dagger}_{\vec{y}t_0,\vec{y}t_0})\rangle\langle\sum_{\vec{x}}\mathrm{Tr}(G_{\vec{x}t,\vec{x}t})\rangle\delta_{\vec{r},0}
\end{aligned}$$

$= $ 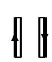 $-$ 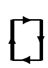 $+\, C_0\,.$ (3.45)

Here the propagator of one quark with a given flavor within each meson was replaced by the corresponding heavy-quark propagator defined in (3.31). Since $G^{(h)}_{\vec{y}t,\vec{x}t_0} \equiv 0$ for $\vec{x} \neq \vec{y}$, the correlation matrix becomes again diagonal.

There are five different contributions to $C^{(4)}$ in this case. The first term corresponds to the pure gluon exchange part of the interaction. The second term corresponds to an interaction involving light valence quark exchange. The last three terms contribute to the four-point correlator only for distance $\vec{r} = 0$. Their overall contribution is denoted by C_0 in the schematic representation in the last line of (3.45). The meson-antimeson energies $W(r)$ can be extracted from the asymptotic time behavior of $C^{(4)\mathrm{M\bar{M}}}_{r,I=1}$ at a given r, and the interaction potential is again defined as in (3.38).

3.4.2 $\mathrm{M\bar{M}}$ Gluon-Exchange Potentials

Unfortunately the lattice simulation of the $\mathrm{M\bar{M}}$ system is problematic due to the appearance of the valence-quark exchange diagram in (3.45) (see discussion in Section 3.4.4). Therefore for computational reasons as a first step only the direct, i.e. pure gluon-exchange term

$$C^{(4\mathrm{d})}_{\vec{r}}(t,t_0) = \frac{1}{V^2}\langle \sum_{\vec{x}} \mathrm{Tr}(G^{(h)\dagger}_{\vec{x}+\vec{r}t,\vec{x}+\vec{r}t_0} G_{\vec{x}+\vec{r}t,\vec{x}+\vec{r}t_0})\,\mathrm{Tr}(G^{(h)}_{\vec{x}t,\vec{x}t_0} G^{\dagger}_{\vec{x}t,\vec{x}t_0})\rangle \quad (3.46)$$

is computed. The knowledge of the gluon-exchange contribution may already give more insight into the nature of $\mathrm{M\bar{M}}$ interactions.

One can easily verify that despite the strong similarity between the direct terms of the MM and $\mathrm{M\bar{M}}$ interactions, the two contributions are not identical. Let us write

$$\begin{aligned} G^{(h)ab}_{\vec{x}+\vec{r}t,\vec{x}+\vec{r}t_0} &= A_1 + iB_1\,, \quad G^{(h)cd}_{\vec{x}t,\vec{x}t_0} = A_2 + iB_2\,, \\ G^{ab}_{\vec{x}+\vec{r}t,\vec{x}+\vec{r}t_0} &= a_1 + ib_1\,, \quad G^{cd}_{\vec{x}t,\vec{x}t_0} = a_2 + ib_2\,. \end{aligned}$$

Thus according to (3.46) the direct term of the $\mathrm{M\bar{M}}$ interaction is formally

$$(A_1 - iB_1)(a_1 + ib_1)(A_2 + iB_2)(a_2 - ib_2)\,,$$

whereas for the direct term of the MM correlator (3.33) we obtain

$$(A_1 + iB_1)(a_1 - ib_1)(A_2 + iB_2)(a_2 - ib_2)\,,$$

which is different from the $\mathrm{M\bar{M}}$ case.

The quenched simulation was performed on an $N_s^3 \times N_t = 8^3 \times 16$ lattice with the inverse gauge coupling $\beta = 5.6$ and light-quark masses $m_f a = 0.1$ and 0.05. Again the results were obtained from an analysis of 100 configurations separated by 200 updates of the gauge fields. The inversion of the fermionic matrix was performed with 32 random sources.

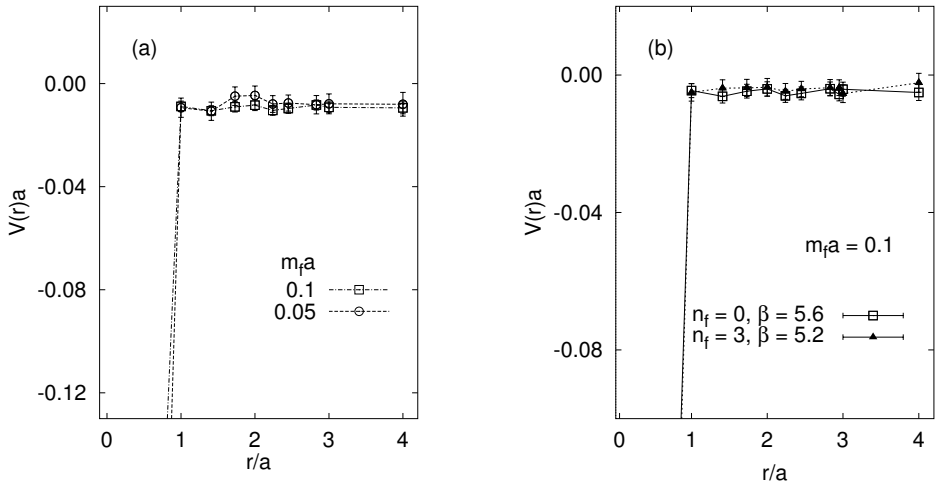

Figure 3.16: (a) Heavy-light meson-antimeson potentials $V(r)$ corresponding to the direct term for different light-quark masses m_f. Lines are to guide the eye. (b) Same for quark mass $m_f a = 0.1$, comparing the quenched simulation with $\beta = 5.6$ and a full QCD simulation with $\beta = 5.2$ and number of flavors $n_f = 3$.

The meson-antimeson energies $W(r)$ were extracted from $C_r^{(4\mathrm{d})}$ using the fit function (3.40) with $n = 1$ (four-parameter fit). To have the averages over the same configurations with the same statistical errors, the mass of two non-interacting (anti)mesons was also extracted from fits to the square of the meson two-point function $[C^{(2)}]^2$, where the correlator $C^{(2)}$ is given in (3.32).

The resulting potentials $V(r)$ for different light-quark mass parameters are shown in Fig. 3.16(a). At distance $r = 0$ we obtain an attractive potential $V(0)a \simeq -0.662$ for $m_f a = 0.1$ and $V(0)a \simeq -0.956$ for $m_f a = 0.05$ (not shown in the figure) being much stronger than for the MM case. The cluster values are reached already at $r/a = 1$. Gluon exchange seems to play an important role only for very short distances.

In order to elucidate how significant the contribution of dynamic quarks to the direct term is, a full QCD investigation of (3.46) was performed by using the pseudo-fermionic method for the simulation of the dynamic fermions. The number of flavors was set to $n_f = 3$, with the dynamic quark mass $m_q a = 0.1$. Recall that the choice of a coupling $\beta = 5.2$ leads to

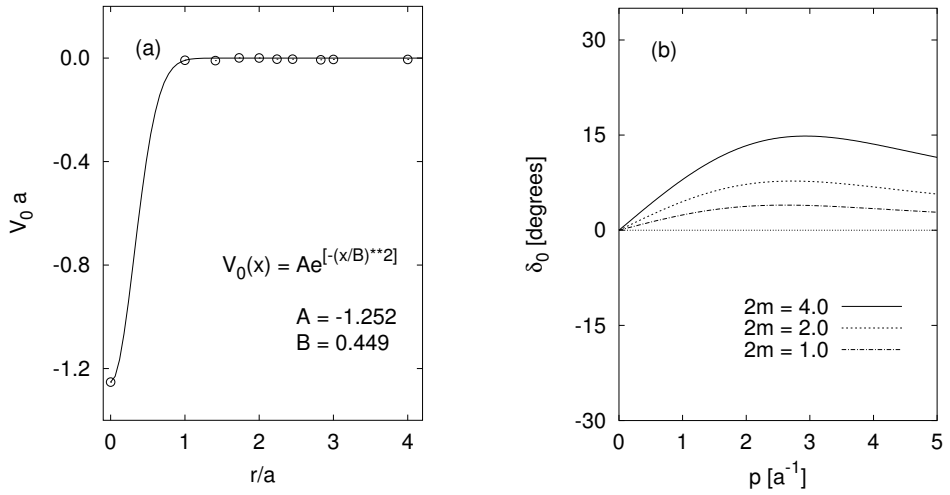

Figure 3.17: $M\bar{M}$ gluon-exchange potential from the simulation data in Fig. 3.16(a) extrapolated to the chiral limit (a), together with the resulting phase shifts δ (b).

a lattice constant comparable with that of the quenched simulation. The results with and without dynamic quarks for light valence-quark mass parameter $m_f a = 0.1$ are presented in Fig. 3.16(b). Similarly to the MM case, the quenched and unquenched results are the same within statistical errors, suggesting that the influence of (relatively heavy) dynamic quarks is not considerable.

Like in the meson-meson case, a linear extrapolation of the data for the two different light-quark masses in Fig. 3.16(a) was performed towards the chiral limit, in order to get closer to the physical masses of the light quarks. By making a two-parameter fit to the resulting data points using a Gaussian function, an analytic form for the interaction potential was obtained which is shown in Fig. 3.17(a). The interaction potential was then used as an input to the Schrödinger equation for a phase shift calculation. The resulting phase shifts are displayed in Fig. 3.17(b) with three arbitrary values of the meson mass.

3.4.3 $I = 0$ M$\bar{\text{M}}$-Potentials from Lattice and Inverse Scattering

A desirable next step in our program would be to compare our lattice QCD results with the experiment. Unfortunately the interactions between mesons having one heavy flavor are known very poorly. Our knowledge of the meson-meson interactions is based mainly on reactions in which $\pi\bar{\pi}$ or $K\bar{K}$ pairs are produced. The production processes of the scalar mesons f_0 and a_0 (which both decay into $K\bar{K}$ pairs) have been studied in many experiments [67, 68]. From the analysis of the experimental data information about $K\bar{K}$ scalar-isoscalar phase shifts has been extracted [69].

To make a comparison with our M$\bar{\text{M}}$ potentials, in principle one has to obtain a simple potential operator $V_L(r)$ from experimentally known phase shifts $\delta_L(k)$ for a given equation of motion. Such an operator may be calculated by inverse scattering theory [70, 71].

Because the experimental information is limited to a certain energy interval, the inverse problem is ill-posed and one has to regularize it, i.e. one has to interpolate and extrapolate the phase shifts for all energies in the smoothest possible way, obeying the proper behavior at low and highest energies. Thus any meaningful application of the potential obtained in this way is limited to a domain where genuine data are used.

The experimental situation for low energy $K\bar{K}$ scattering was parametrized with an effective range expansion by Kaminski and Lesniak [72]. Their expansion is valid at low energy and, unfortunately, takes inelasticities not into account. Nevertheless it is the only available experimental information used in an inversion scheme, and since also in the lattice QCD case no inelastic channels are considered, a comparison of the results is interesting.

Kaminski and Lesniak [72] give two sets of parameters for the effective range expansion

$$k \cot \delta_K(k) = \frac{1}{\text{Re } a_K} + \frac{1}{2} R_K k^2 + V_K k^4 + \mathcal{O}(k^6)\,, \tag{3.47}$$

which are documented in Table 3.1. Based on these parameters, Sander and von Geramb [65, 66] calculated the phase shifts $\delta_0(M_{K\bar{K}})$ shown in Fig. 3.18(b). These phase shifts were then used as input for a standard rational Gelfand–Levitan–Marchenko inversion program [70, 71].

The real local and energy independent inversion potentials are describing purely elastic $K\bar{K}$ scattering. Coulomb effects are not included. The result is shown in Fig. 3.18(a). The reproduction of the effective range parameters

Model	Re a_K [fm]	R_K [fm]	V_K [fm^3]
Set 1	-1.73	0.38	-0.66
Inversion	-1.73	0.38	
Set 2	-1.58	0.20	-0.83
Inversion	-1.58	0.20	

Table 3.1: $K\bar{K}$ isoscalar scattering lengths from [72] and their reproduction by inversion potentials.

is given in Table 3.1 and the phase shift reproduction is demonstrated in Fig. 3.18(b).

The correlator defined in (3.45) corresponds to an $\mathrm{M\bar{M}}$ system in the $I = 1$ channel. To have the agreement between the quantum numbers of the lattice mesons and the inversion results one has to couple the $\mathrm{M\bar{M}}$ dynamics to the scalar $I = 0$ channel. This can be achieved by inserting the fields

$$\begin{aligned}\Phi^{\mathrm{M\bar{M}}}_{\vec{r},I=0}(t) &= (\sqrt{2}V)^{-1}\sum_{\vec{x}}\sum_{\vec{y}}\delta_{\vec{r},\vec{y}-\vec{x}}\Big[\\ &\quad \phi^{\bar{K}0}_{\frac{1}{2}+\frac{1}{2}}(\vec{x}t)\phi^{K0}_{\frac{1}{2}-\frac{1}{2}}(\vec{y}t)+\phi^{K0}_{\frac{1}{2}-\frac{1}{2}}(\vec{x}t)\phi^{\bar{K}0}_{\frac{1}{2}+\frac{1}{2}}(\vec{y}t)\\ &- \phi^{K^+}_{\frac{1}{2}+\frac{1}{2}}(\vec{x}t)\phi^{K^-}_{\frac{1}{2}-\frac{1}{2}}(\vec{y}t)-\phi^{K^-}_{\frac{1}{2}-\frac{1}{2}}(\vec{x}t)\phi^{K^+}_{\frac{1}{2}+\frac{1}{2}}(\vec{y}t)\Big] \qquad (3.48)\end{aligned}$$

into the defining formula of the four-point correlator (3.23) and performing the contractions. Here the fields ϕ of the meson-antimeson partners are defined as in (3.20) and (3.43), with different light-quark flavors for the $K_0\bar{K}_0$ and K^+K^- cases. The resulting four-point correlator consists of 96 different terms but simplifies radically if we take $m_u = m_d$, and replace the propagators of the s quarks with the heavy-quark propagators defined in (3.31). We obtain:

$$\begin{aligned}C^{(4)\mathrm{M\bar{M}}}_{\vec{r},I=0}(t,t_0) &= \frac{4(1+\delta_{\vec{r},0})}{V^2}\Big\langle\sum_{\vec{x}}\mathrm{Tr}(G^{(h)\dagger}_{\vec{x}+\vec{r}t,\vec{x}+\vec{r}t_0}G_{\vec{x}+\vec{r}t,\vec{x}+\vec{r}t_0})\\ &\times\ \mathrm{Tr}(G^{(h)}_{\vec{x}t,\vec{x}t_0}G^{\dagger}_{\vec{x}t,\vec{x}t_0})\Big\rangle\\ &- \frac{8\delta_{\vec{r},0}}{V^2}\Big\langle\sum_{\vec{x},\vec{y}}(-1)^{\sum_\mu(x_\mu+y_\mu)}\mathrm{Tr}(G^{\dagger}_{\vec{x}t,\vec{y}t_0}G_{\vec{x}t,\vec{y}t_0})\Big\rangle\\ &= \quad - \quad . \qquad (3.49)\end{aligned}$$

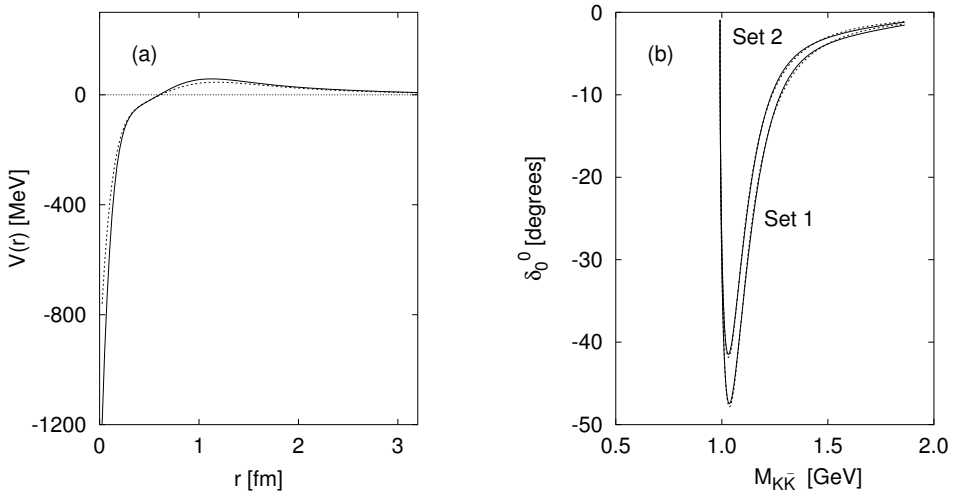

Figure 3.18: (a) $K\bar{K}$ $L = 0$ real isoscalar potentials from quantum inversion based on the two sets of parameters given by Kaminski and Lesniak [72] (Set 1: full line, Set 2: dashed). (b) $K\bar{K}$ $L = 0$ real isoscalar phase shifts calculated from the effective range expansion (dashed) and their reproduction by the inversion potentials (full line).

The first term is the direct gluon-exchange term discussed in the previous section. The second term corresponds to the propagation of a scalar light meson, after a heavy quark-antiquark annihilation, contributing only for distance zero.

One has to be aware of a systematic error in the second contribution to the four-point correlator (3.49)

$$C_2 = -\frac{8\delta_{\vec{r},0}}{V^2}\Big\langle \sum_{\vec{x},\vec{y}} (-1)^{\sum_\mu (x_\mu + y_\mu)} \,\mathrm{Tr}(G_{\vec{x}t,\vec{y}t_0} G^\dagger_{\vec{x}t,\vec{y}t_0})\Big\rangle \tag{3.50}$$

$$= -\frac{8\delta_{\vec{r},0}}{V^2}\Big\langle \sum_{\vec{x}\vec{y}} \sum_{ab} (-1)^{\sum_\mu (x_\mu + y_\mu)} \,|G^{ab}_{\vec{x}t,\vec{y}t_0}|^2\Big\rangle , \tag{3.51}$$

if one uses only a single set of random sources for the calculation of all quark propagators. With a finite number of random sources N_R, Eq. (3.9) provides an approximation $\widetilde{G}$ that deviates from the true quark propagator matrix element G by a random noise error E, with $\langle E \rangle = 0$:

$$\widetilde{G}^{ab}_{\vec{x}t,\vec{y}t_0} = G^{ab}_{\vec{x}t,\vec{y}t_0} + E^{ab}_{\vec{x}t,\vec{y}t_0} \ . \tag{3.52}$$

Thus in (3.51) we have contributions like

$$\begin{aligned} |\widetilde{G}^{ab}_{\vec{x}t,\vec{y}t_0}|^2 &= |G^{ab}_{\vec{x}t,\vec{y}t_0}|^2 \\ &+ (E^{ab}_{\vec{x}t,\vec{y}t_0} G^{ab*}_{\vec{x}t,\vec{y}t_0} + E^{ab*}_{\vec{x}t,\vec{y}t_0} G^{ab}_{\vec{x}t,\vec{y}t_0}) + |E^{ab}_{\vec{x}t,\vec{y}t_0}|^2 . \end{aligned} \tag{3.53}$$

The second term gives zero contribution in the statistical average, but the third term does not. To eliminate this systematic error from the correlator one has to use two different sets of random vectors when evaluating the quark propagators. This is realized by calculating N_R random vectors with the conjugate gradient method, and then using the first half of the ensemble to approximate the first propagator in (3.50) and the second half to generate the second one

$$\begin{aligned} C_2 &= -\frac{8\delta_{\vec{r},0}}{V^2} \Big\langle \sum_{\vec{x}\vec{y}} \sum_{ab} (-1)^{\sum_\mu (x_\mu + y_\mu)} \frac{1}{N_R/2} \sum_{i=1}^{N_R/2} I^{(t_0)}_{i,a}(\vec{x},t) R^{*(t_0)}_{i,b}(\vec{y}) \cdot \\ &\quad \Big(\frac{1}{N_R/2} \sum_{j=N_R/2+1}^{N_R} I^{(t_0)}_{j,a}(\vec{x},t) R^{*(t_0)}_{j,b}(\vec{y}) \Big)^* \Big\rangle . \end{aligned} \tag{3.54}$$

The correlator in (3.49) was computed in a quenched lattice QCD simulation by using the same parameters as in the simulation of the direct term, with $m_f a = 0.1$. The resulting potentials are presented and compared with the direct gluon-exchange potentials in Fig. 3.19. As expected, for non-zero distances the potentials are the same within statistical errors. For distance zero, the potential in the $I = 0$ channel is less deep due to the heavy-quark annihilation term.

The potential obtained by the inversion (Fig. 3.18) is strongly attractive for very short distances. This is in agreement with the simulation results presented in Fig. 3.19. The strength of the lattice potentials at distances close to 0 is weaker but may increase in the chiral limit. The $K\bar{K}$ inversion potential, however, is of longer range and exhibits a slightly repulsive bump at intermediate distances, a feature that could not be resolved by the QCD simulation. The phase shifts computed from the simulation signal the absence of a bound state already for the deeper direct gluon-exchange potentials, whereas the experimental phase shifts hint at its existence. This difference might be due on one hand to the approximations used in the lattice simulation and on the other hand to the lack of precise and complete experimental data for the inversion.

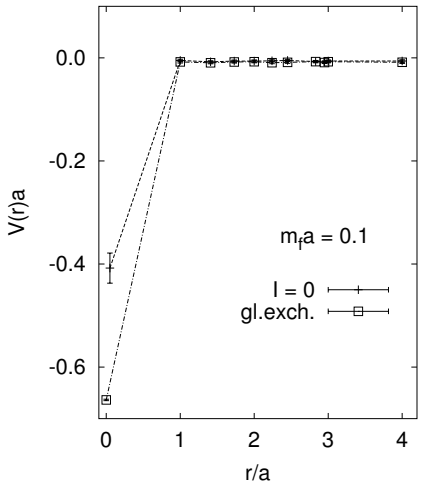

Figure 3.19: $\mathrm{M\bar{M}}$ potential in the $I = 0$ channel for light-quark mass $m_f a = 0.1$, compared to the direct gluon-exchange potential for the same m_f from Fig. 3.16(a).

3.4.4 $I = 1$ $\mathrm{M\bar{M}}$-Potentials

The four-point correlator describing the dynamics of the $I = 1$ $\mathrm{M\bar{M}}$ system is given in (3.45). The lattice simulation of this correlator requires higher CPU time due to new technical solutions in the computation of the valence-quark exchange diagram. In order to evaluate this term one has to compute quark propagators of the type $G(t, t)$. With the random source technique used by us only propagators of the type $G(t, t_0)$ are obtained, with fixed t_0 (see Section 3.1.1). Thus in order to get all possible propagators $G(t, t)$ in principle one has to perform the fermionic matrix inversion N_t times by using in (3.3) N_t different sets of sources of the type (3.5) which are successively non-zero on different time slices $t_0 \in \{1, \ldots, N_t\}$. Regarding the cost of the simulation this means an N_t-fold increase in CPU time.

In principle all-to-all propagators can be obtained also by replacing the sources (3.5) by sources that are non-zero on all time slices

$$Y_{i,a}(\vec{x}, x_4) = R_{i,a}(\vec{x}, x_4) \ , \tag{3.55}$$

where the complex random vectors R satisfy the relation

$$\frac{1}{N_R}\sum_{i=1}^{N_R} R^*_{i,a}(\vec{x},x_4)R_{i,b}(\vec{y},y_4) = \delta_{\vec{x},\vec{y}}\,\delta_{x_4,y_4}\delta_{a,b}\ . \tag{3.56}$$

With this choice of random sources, however, one does not impose an exact delta function for the time coordinate, as a result of which the exponential fall-off in time of the correlators will be affected, causing difficulties in the extraction of interaction potentials. Note that all propagators which do not have the form $G(t,t_0)$ are of the type $G(t,t)$, i.e. start and end on the same time slice t. This observation may help in the evaluation of the valence-quark exchange diagram. A plausible trick which comes to mind is to determine the propagators $G(t,t_0)$—which ultimately determine the fall-off of the correlators—in the usual way, and to use the sources (3.55) in a subsequent inversion of the fermionic matrix to determine the propagators $G(t,t)$. Such a procedure means only a two-fold increase in CPU time, and thus a remarkable improvement compared to the other method.

The correlator in (3.45) was computed in quenched lattice QCD with the same parameters as in the previous simulations. All five terms were taken into account. The light-quark propagators were calculated by both methods presented above. In the case with $N_t = 16$ sets of random sources only 50 configurations were generated because of the huge CPU demand. The resulting interaction potentials are presented in Fig. 3.20. The two different methods yield the same results within statistical errors. The potential is attractive for $r/a = 1$, whereas for larger separations the interaction is compatible with zero. A comparison with the gluon-exchange potentials from the direct diagram in Fig. 3.16 shows that the valence-quark exchange diagram yields an attraction of longer range. This term includes pion-exchange contributions even in the quenched approximation as demonstrated in Fig. 3.21. The big error bars at distance $r = 0$ are a consequence of the accumulation of the uncertainties of the five different terms contributing to $C^{(4)\mathrm{M}\bar{\mathrm{M}}}_{r=0,I=1}$.

Comparing Figs. 3.20 and 3.9 it turns out that the $I = 1$ $\mathrm{M}\bar{\mathrm{M}}$ potentials are approximately of the same range as the $I = 1$ MM potentials, but they are much more attractive. In order to examine the possibility of the formation of bound $\mathrm{M}\bar{\mathrm{M}}$ states, a further quantum-mechanical analysis is desirable. Such an analysis requires an analytic form for the interaction potential. Obviously, the strength of the potential at $r = 0$ is decisive for the determination of such an analytic form and ultimately for the existence or non-existence of a bound resonant state. Because of the large uncertainty

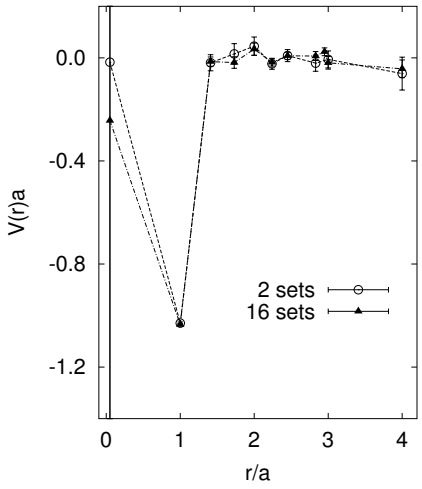

Figure 3.20: $M\bar{M}$ potentials in the $I = 1$ channel for light-quark mass $m_f a = 0.1$, comparing simulations with 2 and 16 sets of random vectors to evaluate the light-quark propagators (see text).

at distance zero, we made two different fits to the data points from the simulation with 2 sets of random sources using a Gaussian and a Saxon-Woods function. They are shown in Figs. 3.22(a) and 3.22(b), respectively. These analytic forms for the potentials were then used as inputs for a standard resonant state search program [62]. A resonant meson-antimeson state was not found for either of the potentials. Further variations of the parameters of the potentials show that the strength parameters A can be tuned in a wide range—up to a factor two in the more favorable case of the Saxon-Woods potential—without obtaining a stable resonant state. The reason is that the width of the potential well is not large enough. Indeed, increasing e.g. the diffuseness parameter of the Saxon-Woods potential to $B = 2$ already leads to a negative ground state energy. To conclude, our lattice calculations give evidence that exotic mesons consisting of a heavy-light meson and its antiparticle in the $I = 1$ channel do not exists. However, more statistics is needed at least for distance $r = 0$.

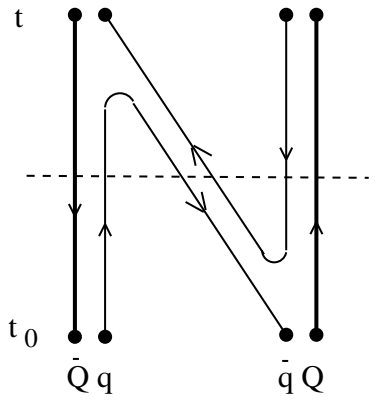

Figure 3.21: A pion-exchange contribution from the valence-quark exchange term of the $I = 1$ $M\bar{M}$ propagator. At the time slice indicated by the dotted line, two heavy-light (anti)mesons and a pion are present.

3.5 Simulations with an Improved Action

Realistic lattice simulations necessitate large computer times. The lattice spacing a is the most important determinant of the cost. For example, with the best algorithms the cost of a full QCD simulation increases like $1/a^6$ as a is decreased. This suggests that one should keep a as large as possible. On the other hand, finite lattice spacings introduce systematic errors of lattice simulations. Until recently there was a general belief that lattice spacings of order $0.05 - 0.1$ fm or less were necessary for accurate simulations. With the development of two new approaches to the design of improved actions and operators [73, 74] reliable results can be obtained for lattice spacings as large as 0.4 fm. The computational advantage of coarse lattices is enormous and will certainly redefine numerical QCD: the simplest calculations can be done on a personal computer, while problems of unprecedented difficulty and precision can be tackled with large supercomputers. Therefore these improvement techniques can be considered as one of the most important achievements of the last years in lattice QCD.

The idea of utilizing improved actions in our computations of hadron-hadron interactions on the lattice comes from the following observations:

i) The residual hadronic forces are $10^{-2} - 10^{-3}$ times smaller than a typical hadron mass, whereas the most precise unimproved lattice simulations can reproduce the low-energy properties of hadrons to within a few percent, i.e. the effect to be studied has the same order of magnitude as the inherent

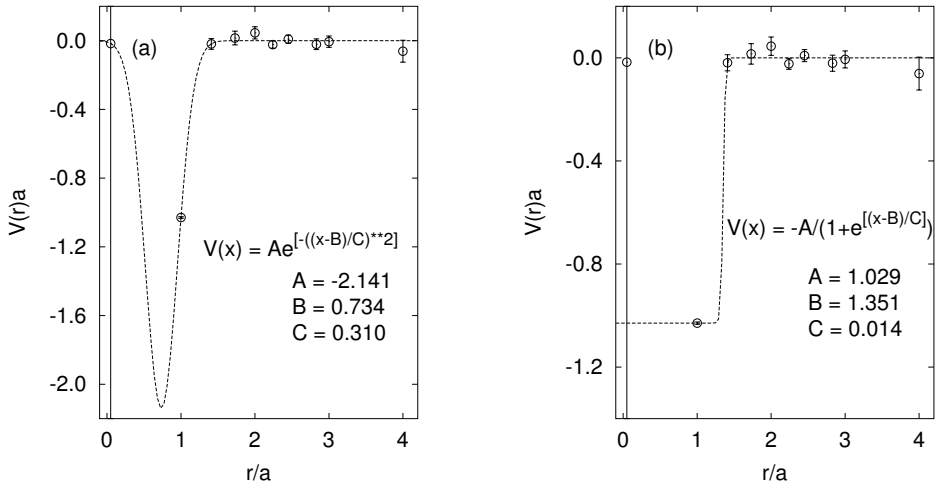

Figure 3.22: Fits to the $M\bar{M}$ potentials in Fig. 3.20 with a Gaussian (a) and a Saxon-Woods (b) function.

error. The utilization of improvement techniques leading to higher precision is therefore highly desirable.

ii) To have a clearer shape of the potentials, non-integer (off-axes) separations $r/a = \sqrt{2}, \sqrt{3}$, etc. were also considered when computing the meson-meson energies $W(r)$. The resulting MM and $M\bar{M}$ potentials in Figs. 3.9 and 3.16 exhibit systematic deviations, which may originate from anisotropy effects of the cubic lattice. Simulations using improved lattice actions restore rotational O(3) invariance and may help to estimate these systematic errors on $W(r)$.

iii) Although the lattices we used so far seem to be large enough to accommodate a two-meson system, studies of interactions between light hadrons [51] already indicate the necessity of simulations on larger physical volumes. Since lattices with more lattice points have numerical limits, the only way to obtain a physically larger lattice volume is to increase the lattice constant a.

We use the improvement technique developed by Lepage and coworkers [74] which is based on Symanzik's idea [75] to introduce new terms into the lattice action in order to improve the discretization of the derivatives and to reintroduce the contribution of the $k > \pi/a$ states excluded by the lattice. The coefficients of these terms are then computed in lattice perturbation

theory using a prescription for removing tadpole contributions [76]. In the following we give a brief overview of this improvement technique and present simulation results for the MM and M$\bar{\text{M}}$ systems obtained with an improved gluonic action.

3.5.1 Improved Actions and Operators

Replacing space-time by a discrete lattice is an approximation. A non-zero lattice spacing results in two types of error: the error that arises when we replace derivatives in the field equations by finite-difference approximations, and the error due to the ultraviolet cutoff imposed by the lattice. Both types of errors can be reduced by including terms of higher order in a into the action.

It has been shown that at the classical level $\mathcal{O}(a^2)$ errors due to the finite-difference approximations can be removed by adding a term with six-link rectangular plaquettes

$U_{\rm rt} =$ 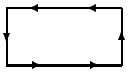

to the usual Wilson gauge field action (2.54) [77–79]. A significant improvement is obtained by introducing tadpole factors in the six-link term [76]. Their role is to cancel the large renormalizations that arise from tadpole diagrams specific to lattice QCD. Thus the form of the tree level tadpole improved action is

$$S_{\rm G}[U] = \beta_{\rm pl} \sum_{\rm pl} \left(1 - \frac{1}{3} \,\mathrm{Re}\,\mathrm{Tr}\, U_{\rm pl}\right) + \beta_{\rm rt} \sum_{\rm rt} \left(1 - \frac{1}{3} \,\mathrm{Re}\,\mathrm{Tr}\, U_{\rm rt}\right), \qquad (3.57)$$

where $U_{\rm pl}$ is the plaquette operator from (2.53). The coupling parameter $\beta_{\rm rt}$ is related to the input coupling $\beta_{\rm pl}$ via

$$\beta_{\rm rt} = -\frac{\beta_{\rm pl}}{20 u_0^2}, \qquad (3.58)$$

where the mean link u_0 represents nonperturbative corrections for tadpole contributions, and is given in terms of the measured expectation value of the plaquette:

$$u_0 = (\frac{1}{3} \mathrm{Re}\,\mathrm{Tr} \langle U_{\rm pl} \rangle)^{1/4}. \qquad (3.59)$$

The coupling $\beta_{\rm rt}$ is then determined self-consistently with u_0 for a given $\beta_{\rm pl}$.

Tadpole improvement is the first step in a systematic procedure for improving the action. The next step is to add in renormalizations due to contributions from $k > \pi/a$ physics not already included in the tadpole improvement. For example, one-loop corrections would bring a third term into the action in (3.57), but it turns out that their $\mathcal{O}(a^2\alpha_s)$ contribution is comparable to those of $\mathcal{O}(a^4)$ and is therefore relatively unimportant [74].

The complete $\mathcal{O}(a^2)$ improvement of our lattice operators necessitates also the improvement of the fermionic sector. Due to the absence of $\mathcal{O}(a)$ errors for the staggered fermion action [80] and the complexity of the staggered formalism, its $\mathcal{O}(a^2)$ improvement has received little attention. Almost ten years ago, Naik proposed adding a third-nearest-neighbor term to the standard staggered fermion action to remove some $\mathcal{O}(a^2)$ effects [81]. Recently it has been shown, that two counterterms are needed to construct the $\mathcal{O}(a^2)$ on-shell improved staggered fermionic action [82], which at tree level reduces to the Naik action

$$\begin{aligned} S_{\mathrm{F}} \;=\; & \sum_{x,\mu} \Gamma_{x\mu} \bar{\chi}_x \Big\{ \frac{9}{16} \Big[U_{x\mu} \chi_{x+\hat{\mu}} - U^{\dagger}_{x-\hat{\mu},\mu} \chi_{x-\hat{\mu}} \Big] \\ & - \frac{1}{48} \Big[U_{x\mu} U_{x+\hat{\mu},\mu} U_{x+2\hat{\mu},\mu} \chi_{x+3\hat{\mu}} - U^{\dagger}_{x-\hat{\mu},\mu} U^{\dagger}_{x-2\hat{\mu},\mu} U^{\dagger}_{x-3\hat{\mu},\mu} \chi_{x-3\hat{\mu}} \Big] \Big\} \\ & + m \sum_x \bar{\chi}_x \chi_x \; . \end{aligned} \tag{3.60}$$

The improvement of the fermionic sector leads to a modified fermionic matrix including more off-diagonal terms. The inversion of such a matrix needs approximately a factor of 10 more CPU time. Preliminary runs using the improved fermionic action (3.60) showed little difference from the outcome of the simulation results with the original Kogut-Susskind action (2.52). Thus for computational reasons the new simulations were performed using the improved gauge action (3.57) and leaving the fermionic sector unchanged.

The simulation with the improved gluonic sector is computationally more demanding than a normal run, if one wants to use the same lattice spacing. The reason is that there are more 2×1 rectangles than 1×1 plaquettes involved in a Monte Carlo upgrade for a given link. According to Fig. 3.23, there are 6 rectangles containing the link into consideration in a given plane, so altogether there are $6 \times 3 = 18$ such rectangles in the 3 perpendicular planes containing the link, compared to only 6 plaquettes for the normal run. Since the computation of the rectangles is also more costly than that of the plaquettes, there is an overall 4-fold increase in the CPU time needed for one MC upgrade.

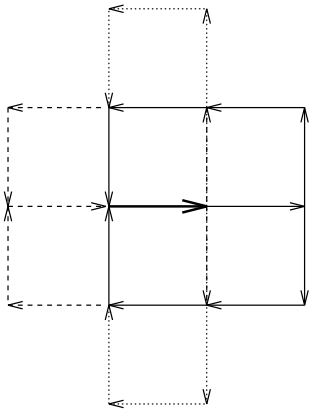

Figure 3.23: Six-link planar rectangles involved in the Monte Carlo upgrade of a given link.

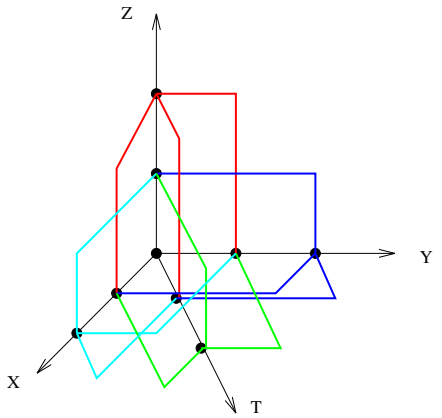

Figure 3.24: All possible six-link rectangles starting from a site and going in positive directions.

The mean link u_0 is computed numerically by guessing a value of β_{rt} for use in the action, measuring the mean link in a simulation, and then readjusting the value of β_{rt} used in the action accordingly. This tuning cycle converges rapidly to selfconsistent values, and can be done very quickly on small lattice volumes, because u_0 depends practically only on the lattice spacing. As an example, in Fig. 3.25 we show the values of the mean plaquette, the mean rectangle and the coupling $\beta_{\rm rt}$ from successive simulations on a 6^4 lattice with input coupling $\beta_{\rm pl} = 6.2$. Note that the computation of the mean rectangle $\frac{1}{3}\mathrm{Re}\,\mathrm{Tr}\langle U_{\rm rt}\rangle$ implies the evaluation of 12 different rectangles for a given site, as shown in Fig. 3.24, whereas only 6 plaquettes are needed for the computation of the mean plaquette. The expectation values were obtained from a measurement on 100 successive configurations. To equilibrate the system 100 iterations with the new $\beta_{\rm rt}$ were allowed. One can see, that the curves reach their plateaus already after the third or fourth run.

3.5.2 Numerical Results for the MM and M$\bar{\rm M}$ Systems

Our earlier results suggest that the lattices we used are reasonably big to accommodate the two-meson system. Instead of increasing the physical volume of the lattice by employing a larger lattice spacing a we performed improved simulations on lattices with the same lattice constant $a \simeq 0.2\,\mathrm{fm}$ and space-time extension $8^3 \times 16$. We were mainly interested to estimate systematic

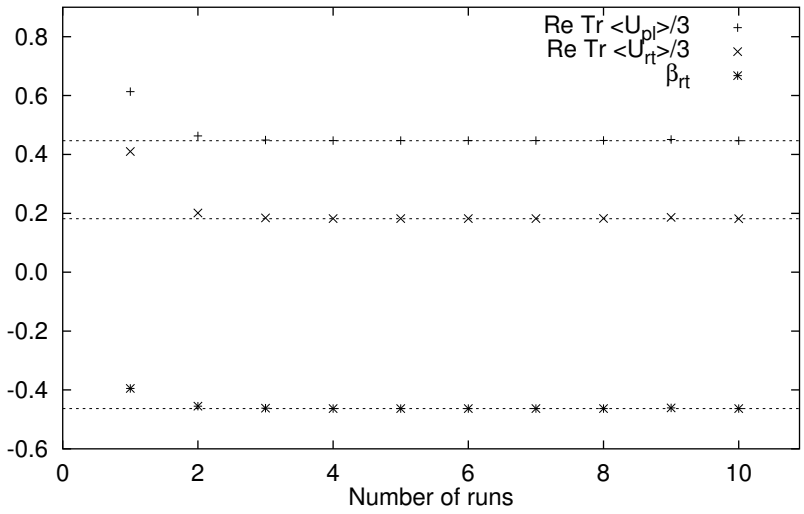

Figure 3.25: Values of the mean plaquette $\frac{1}{3}\mathrm{Re}\,\mathrm{Tr}\langle U_{\mathrm{pl}}\rangle$, the mean rectangle $\frac{1}{3}\mathrm{Re}\,\mathrm{Tr}\langle U_{\mathrm{rt}}\rangle$ and the coupling β_{rt} after successive runs with input coupling $\beta_{\mathrm{pl}} = 6.2$ on a 6^4 lattice. Errors are of the size of the symbols.

errors on our earlier results possibly related to violation of rotational O(3) invariance by the lattice.

There are several ways to match the lattice spacings of the improved and unimproved simulations, like comparing string tensions, hadron masses etc. In our case the coupling β_{pl} of the improved gauge action corresponding to the coupling $\beta = 5.6$ of the original Wilson action was obtained by carrying out a finite-temperature pure QCD simulation on an $8^3 \times 4$ lattice in a search for the confinement-deconfinement phase transition point. Earlier computations show that for systems with the Wilson gauge action the phase transition occurs at $\beta = 5.7$ [51]. In order to locate the phase transition point, several runs were performed using the improved action (3.57) with input values of β_{pl} in the range $6.0 - 8.5$, including tuning cycles to get the u_0 for each value of the input coupling. We used the Polyakov-loop expectation value

$$\langle W \rangle = \Big\langle \frac{1}{V} \sum_{\vec{x}} \mathrm{Tr} \prod_{j=1}^{N_t} U_{x=(\vec{x},ja),\mu=4} \Big\rangle \,, \tag{3.61}$$

as order parameter of the phase transition.

$\beta_{\rm pl}$	$\beta_{\rm rt}$	$\mathrm{ReTr}\langle U_{\rm pl}\rangle/3$	$\mathrm{ReTr}\langle U_{\rm rt}\rangle/3$	$\mathrm{Re}\langle W\rangle^3$	Phase
6.0	-0.460	0.424	0.160	$-1.79{\cdot}10^{-5}$	confined
6.5	-0.465	0.486	0.224	$-2.39{\cdot}10^{-5}$	confined
6.8	-0.466	0.533	0.278	$5.27{\cdot}10^{-5}$	confined
7.0	-0.467	0.560	0.314	$1.57{\cdot}10^{-4}$	confined
7.1	-0.469	0.572	0.328	$3.31{\cdot}10^{-4}$	ph. tranz.
7.2	-0.470	0.587	0.351	$6.44{\cdot}10^{-2}$	deconfined
7.3	-0.472	0.597	0.364	0.148	deconfined
7.6	-0.482	0.621	0.397	0.306	deconfined
7.9	-0.493	0.641	0.425	0.452	deconfined
8.2	-0.505	0.658	0.449	0.666	deconfined
8.5	-0.518	0.673	0.470	0.909	deconfined

Table 3.2: Tuned values of $\beta_{\rm rt}$ for several $\beta_{\rm pl}$ around the temperature phase transition and expectation values of the plaquette, rectangle and Polyakov loop, computed from an average over 100 successive configurations.

In Fig. 3.26 we show the values of W in the complex plane for 100 successive iterations at several couplings $\beta_{\rm pl}$. One can see, that the phase transition occurs between $\beta_{\rm pl} = 7.0$ and $\beta_{\rm pl} = 7.3$. The last three plots nicely signal the spontaneous breaking of Z_3 symmetry in the deconfined phase.

Further simulations in the region $\beta_{\rm pl} = 7.0 - 7.3$ were performed with a finer variation of 0.1 in the coupling. The resulting values of $\beta_{\rm rt}$ as well as the values of the mean plaquette, mean rectangle and the "magnitude" of the Polyakov-loop expectation values $\mathrm{Re}\langle W\rangle^3$ are presented in Table 3.2. Since neither of the operators is a very fluctuating quantity, the expectation values were computed from measurements on just 100 successive configurations, thus they contain autocorrelation effects. The values $\mathrm{Re}\langle W\rangle^3$ for different $\beta_{\rm pl}$ are also shown in Fig. 3.27. The first significantly non-zero Polyakov loop is obtained at $\beta_{\rm pl} = 7.2$. The linear fit in the range $\beta_{\rm pl} = 7.2 - 8.6$ crosses the zero axis at $\beta_{\rm pl} = 7.1$, so we expect that the phase transition occurs near this value of the coupling.

It has to be remarked that the pure SU(3) transition is of first order. The order parameter should undergo a jump or rise steeply. This is not the case for our improved SU(3) simulation and deserves further investigation. The choice of a coupling $\beta_{\rm pl} = 7.0$ with $\beta_{\rm rt} = -0.467$ should roughly corresponds to the same lattice spacing $a \simeq 0.2\,\mathrm{fm}$ as $\beta = 5.6$ of the original simulations with the Wilson gauge action. Thus the couplings of the improved action

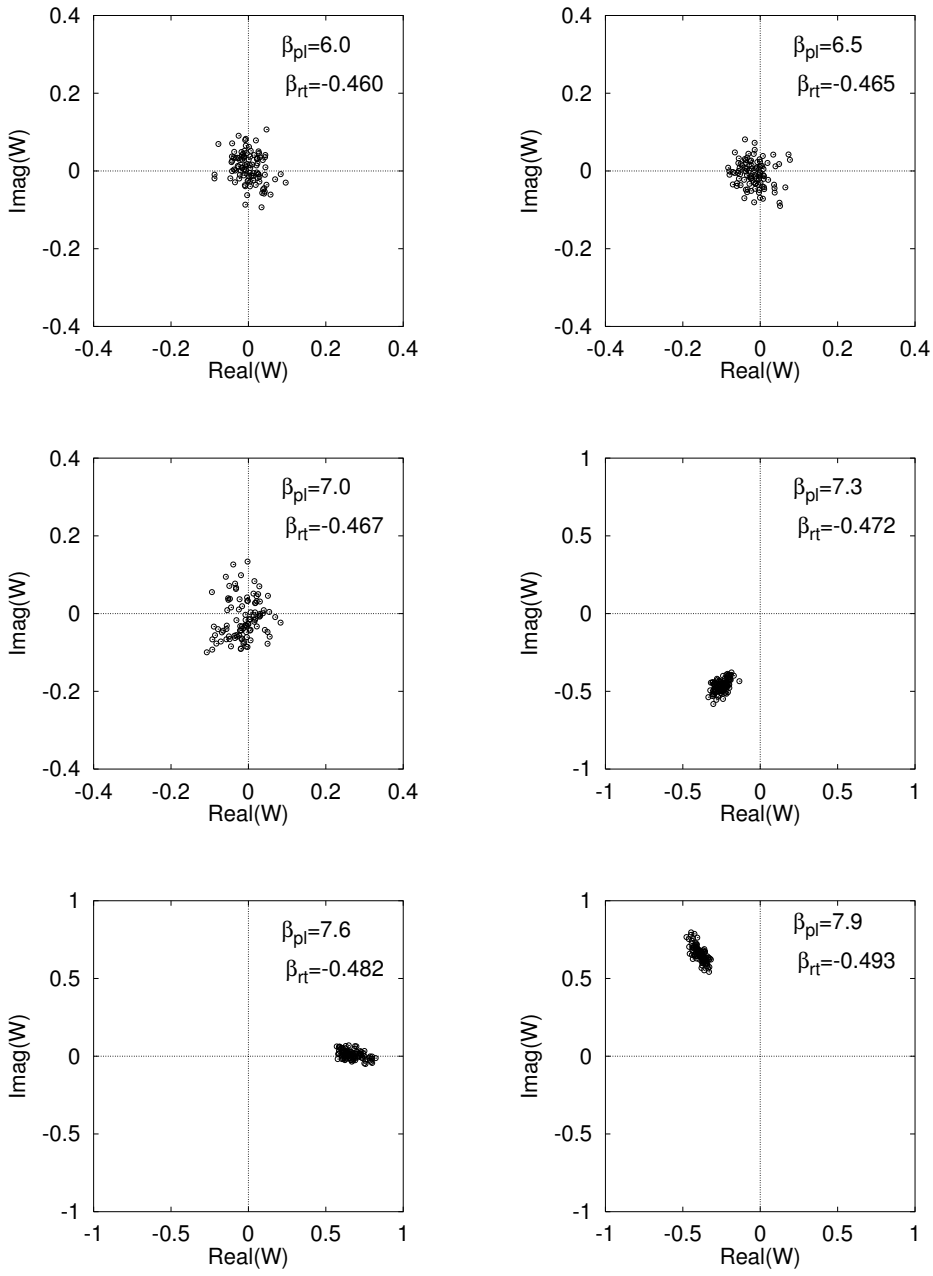

Figure 3.26: Values of Polyakov loops W in the complex plane for 100 successive iterations at different $\beta_{\rm pl}$ in the range $6.0 - 7.9$.

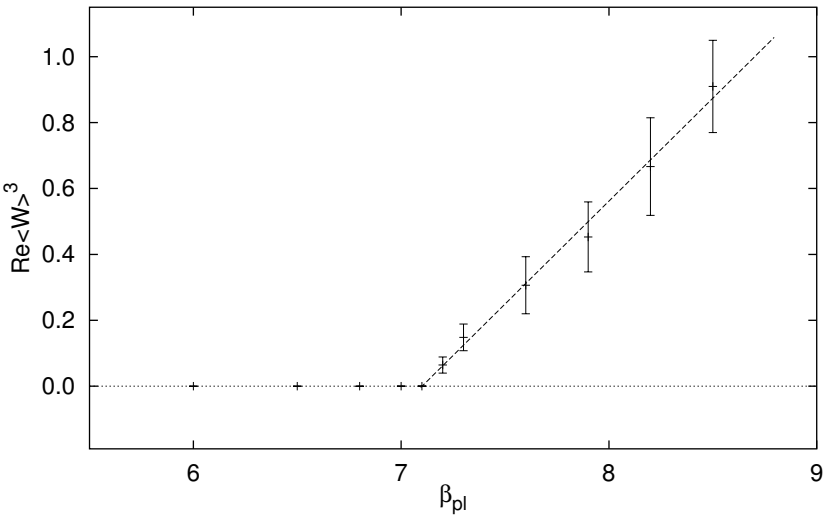

Figure 3.27: Polyakov-loop expectation values $\mathrm{Re}\langle W\rangle^3$ as a funtion of β_{pl} with a linear fit in the range $\beta_{\mathrm{pl}} = 7.2 - 8.6$.

(3.57) were set to these values in the new simulations of the MM and M$\bar{\mathrm{M}}$ systems at zero temperature.

The resulting correlators from the improved simulations are very similar to those from the unimproved simulations. For illustration, the numerical values for $C^{(2)}(t)$ obtained for either case are compared in Table 3.3. To indicate the accuracy of the data, the statistical errors $\Delta C^{(2)}(t)$ are also shown.

The potentials $V(r)a$ for the initial (Wilson) and the improved simulation using the corresponding couplings are compared in Fig. 3.28. In the M$\bar{\mathrm{M}}$ case only the direct gluon-exchange term has been computed. Good agreement is obtained both for integer and non-integer (off-axes) distances. For a better comparison the numerical values for $W(r)a$ are presented in Table 3.4. The systematic shifts of the order $\sim 0.5\%$ are due to the slight difference between the lattice constants, also seen in the $C^{(2)}$ correlator values in Table 3.3. What we learn from these calculations with gluonic improved action is that the anisotropy effects are small. The hump in the MM-potential might be physical.

	Wilson		Improved	
t/a	$C^{(2)}(t)$	$\Delta C^{(2)}$	$C^{(2)}(t)$	$\Delta C^{(2)}$
1	$0.2437 \cdot 10^{0}$	$0.493 \cdot 10^{-3}$	$0.2436 \cdot 10^{0}$	$0.398 \cdot 10^{-3}$
2	$0.6525 \cdot 10^{-1}$	$0.240 \cdot 10^{-3}$	$0.6121 \cdot 10^{-1}$	$0.207 \cdot 10^{-3}$
3	$0.3980 \cdot 10^{-1}$	$0.128 \cdot 10^{-3}$	$0.3967 \cdot 10^{-1}$	$0.113 \cdot 10^{-3}$
4	$0.1371 \cdot 10^{-1}$	$0.661 \cdot 10^{-4}$	$0.1317 \cdot 10^{-1}$	$0.618 \cdot 10^{-4}$
5	$0.6867 \cdot 10^{-2}$	$0.447 \cdot 10^{-4}$	$0.7025 \cdot 10^{-2}$	$0.395 \cdot 10^{-4}$
6	$0.2713 \cdot 10^{-2}$	$0.317 \cdot 10^{-4}$	$0.2645 \cdot 10^{-2}$	$0.301 \cdot 10^{-4}$
7	$0.1232 \cdot 10^{-2}$	$0.195 \cdot 10^{-4}$	$0.1284 \cdot 10^{-2}$	$0.163 \cdot 10^{-4}$
8	$0.1042 \cdot 10^{-2}$	$0.248 \cdot 10^{-4}$	$0.1041 \cdot 10^{-2}$	$0.228 \cdot 10^{-4}$
9	$0.1240 \cdot 10^{-2}$	$0.193 \cdot 10^{-4}$	$0.1274 \cdot 10^{-2}$	$0.188 \cdot 10^{-4}$
10	$0.2721 \cdot 10^{-2}$	$0.300 \cdot 10^{-4}$	$0.2644 \cdot 10^{-2}$	$0.245 \cdot 10^{-4}$
11	$0.6928 \cdot 10^{-2}$	$0.523 \cdot 10^{-4}$	$0.6971 \cdot 10^{-2}$	$0.441 \cdot 10^{-4}$
12	$0.1378 \cdot 10^{-1}$	$0.777 \cdot 10^{-4}$	$0.1314 \cdot 10^{-1}$	$0.667 \cdot 10^{-4}$
13	$0.3964 \cdot 10^{-1}$	$0.145 \cdot 10^{-3}$	$0.3977 \cdot 10^{-1}$	$0.133 \cdot 10^{-3}$
14	$0.6522 \cdot 10^{-1}$	$0.196 \cdot 10^{-3}$	$0.6078 \cdot 10^{-1}$	$0.199 \cdot 10^{-3}$
15	$0.2432 \cdot 10^{0}$	$0.513 \cdot 10^{-3}$	$0.2442 \cdot 10^{0}$	$0.433 \cdot 10^{-3}$

Table 3.3: Correlation functions $C^{(2)}(t)$ and statistical errors $\Delta C^{(2)}$ for different time separations t/a from simulations using the Wilson gauge action ($\beta = 5.6$) and the improved action ($\beta_{\rm pl} = 7.0$, $\beta_{\rm rt} = -0.467$), respectively.

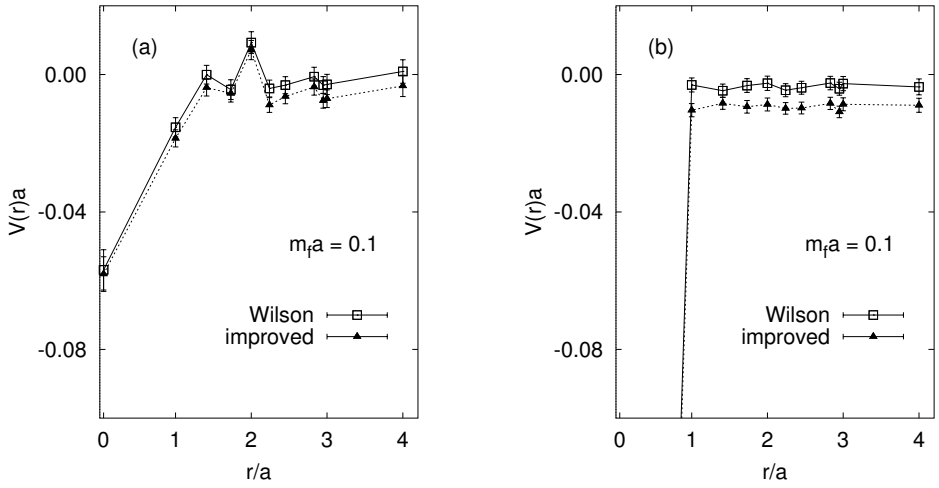

Figure 3.28: MM (a) and M$\bar{\text{M}}$ gluon-exchange (b) potentials $V(r)a$ for quark mass $m_f a = 0.1$, comparing a simulation using the Wilson gauge action with $\beta = 5.6$ and an improved simulation with $\beta_{\rm pl} = 7.0$, $\beta_{\rm rt} = -0.467$ corresponding to the same lattice constant.

	$W(r)a$			
r/a	MM system		M$\bar{\text{M}}$ system	
	Wilson	Improved	Wilson	Improved
0	1.64524	1.64433	1.04336	1.04615
1	1.68674	1.68382	1.69906	1.69202
1.41	1.70205	1.69860	1.69738	1.69403
1.73	1.69771	1.69689	1.69889	1.69300
2	1.71139	1.70952	1.69955	1.69368
2.24	1.69803	1.69353	1.69753	1.69254
2.45	1.69900	1.69601	1.69825	1.69264
2.83	1.70148	1.69876	1.69961	1.69400
3a	1.69902	1.69478	1.69797	1.69151
3b	1.69921	1.69536	1.69946	1.69374
4	1.70298	1.69908	1.69850	1.69345

Table 3.4: Values of $W(r)a$ for the Wilson ($\beta = 5.6$) and improved ($\beta_{\rm pl} = 7.0$) simulation. 3a and 3b are on and off-axis separations $r/a = 3$, respectively.

Chapter 4

Summary and Conclusion

In theoretical nuclear physics there is great interest in a fundamental understanding of hadron-hadron interactions. Today, QCD is believed to be the basic theory of the strong interactions. Since the strong coupling constant becomes large in the low energy regime of this theory, phenomena at nuclear distances are problematic to be treated within perturbation theory. Up to now the most successful non-perturbative tool for a calculation of QCD problems is lattice QCD.

This thesis presents pioneering calculations of hadron-hadron potentials from the basic principles of lattice QCD. A practical method to extract an effective hadron-hadron potential from hadron Green functions has been developed. This method is a transcription of scattering theory from text books to the lattice, and allowed us to take the effect of dynamic valence quarks into account. Because of the huge numerical effort involved in the task of calculating hadron four-point correlation functions on the lattice, as a first step systems of two pseudoscalar mesons were considered. The calculation of baryonic systems has to be postponed to future studies.

In one study we investigated the interaction between two heavy-light mesons. In this approximation the heavy quarks represent static color sources, which localize the mesons and allow in this way the extraction of effective total energies of the two-meson system from the euclidean time behavior of the meson four-point correlation function for various inter-meson distances r. Most of the simulations were performed in quenched lattice QCD with Kogut-Susskind fermions. The resulting potentials turn out to be short ranged and attractive with a range of about 2 lattice spacings or 0.4 fm, and a depth of approximately $0.04 - 0.1$ inverse lattice spacing, or $40 - 100$ MeV

in physical units. Simulations with different light valence-quark masses show that the interaction is stronger for smaller light-quark masses, but its range is always approximately the same. The inclusion of sea quarks did not cause dramatic changes in the potentials. The interaction is obviously driven by gluon exchange. Meson exchange out of the dynamic quark sea seems to play a minor role. A comparison with a simulation on a larger lattice shows that the effect of "mirror" particles is negligible, and that the contributions from excited states do not alter the shape of the potential considerably. An extrapolation to the chiral limit of the potentials for different light-quark masses was performed in order to get closer to physical quark masses. A Gaussian form of the potential was obtained from a two-parameter fit to the resulting data points. This potential was used in a quantum-mechanical study of the behavior of the two-meson system. Despite the attraction for short distances, neither bound nor resonant meson-meson states were found.

In a second study we investigated the interaction between a heavy-light meson and its antiparticle. Pure gluon-exchange potentials for the direct diagram as well as potentials in the $I = 0$ and $I = 1$ channel were computed. In all cases, the meson-antimeson potentials turn out to be attractive and much stronger than the meson-meson potential. The potential in the $I = 0$ channel is of short range—of about 1 lattice spacing or 0.2 fm—and a depth of approximately 0.4 inverse lattice spacing, or 400 MeV. We notice a good qualitative agreement between the simulation results and recent extractions of $K\bar{K}$ potentials from experimental scattering data via inverse scattering theory. The potential in the $I = 1$ channel has a range of about 1.35 lattice spacings or 0.27 fm. Its depth could not be determined because of the large uncertainty of the data point for zero separation. Preliminary quantum-mechanical investigations signal the absence of resonant states also for the meson-antimeson case.

We started implementing improved actions into our computer codes in order to reduce discretization errors, achieve higher precision and make the utilization of larger lattice volumes possible. Results for both the meson-meson and meson-antimeson systems using an $\mathcal{O}(a^2)$ tree-level and tadpole improved gauge action are very close to the unimproved data.

There exists a related study of systems of pion-like light-light mesons in four-dimensional lattice QCD following the same method for the calculation of interaction potentials as used in this thesis. It shows a long ranged interaction between one and five lattice spacings, or $0.2 - 1$ fm, an intermediate attractive regime with a depth of about 0.05 to 0.2 inverse lattice spacings, or 50 to 200 MeV, and a slightly repulsive character below one lattice spacing,

or 0.2 fm [51, 66].

The results obtained in the underlying thesis seem to confirm phenomenology. We expect that a refined analysis, which besides an improved action would include link variable fuzzing and operator smearing in order to enhance the overlap of the interpolating fields with the state with minimal energy, will increase the quality of the data and will ultimately lead to quantitative results. An independent lattice investigation using Wilson fermions is desirable, because the assignment of quantum numbers to the interpolating operators is straightforward, and consequently physical particles are easily identified [83, 84].

Studies similar in spirit to the one initiated here may be extended to various other hadron-hadron systems, like kaon-nucleon for example, for which inversion results exist [65]. Another interesting application would be the question of the stability of the doubly strange spin zero H particle as a $\Lambda\Lambda$ system. Lattice and model studies of this important problem provide conflicting results [85, 86]. The setup of our method makes nuclear physics on the lattice accessible for realistic investigations.

Összefoglalás

Az atommagok nukleonokból épülnek fel. A magfizika többnukleon-rendszerek kötött állapotainak és reakcióinak a vizsgálatával foglalkozik. A többnukleon-rendszert leíró Schrödinger-egyenlet megoldásához szükség van egy nukleon-nukleon potenciál ismeretére. Így az elméleti magfizika egyik legfontosabb feladata a nukleon-nukleon kölcsönhatási potenciál meghatározása. Ebből a célból az utóbbi ötven évben számos fenomenológikus modellt dolgoztak ki. Közülük a legfontosabbakat az első, bevezető fejezetben soroltam fel. Mindegyik modell tartalmaz olyan paramétereket, amelyeket a modellek eredményeinek a kísérleti adatokkal való összevetésével kell beállítani. Így ezek a modellek a nukleáris kölcsönhatás mechanizmusainak csupán kvalitatív megértésére alkalmasak.

A másik fajta hadronok, azaz a mezonok esetén rosszabb a helyzet. A mezon-mezon kölcsönhatásokra vonatkozó kísérleti adatok igen hiányosak, ezért hasonló fenomenológikus modellek megalkotására eddig nem is nagyon került sor. Így felmerül az a gondolat, hogy mind a nukleonok, mind a mezonok közötti kölcsönhatásokat közvetlenül első alapelvekből kiindulva határozzuk meg.

A kísérleti eredmények, valamint az elméleti megfontolások arra mutatnak, hogy a hadronok még elemibb részecskékből, kvarkokból felépülő kompozit részecskék. A kvarkok közötti erős kölcsönhatást a kvantumszíndinamika (QCD) írja le. Az elmélet csatolási állandója alacsony energiákon naggyá válik, ezért ez az ,,erős kölcsönhatás" perturbatív eszközökkel nem kezelhető. A legeredményesebb nemperturbatív leírást a QCD rácson való megfogalmazásával nyerjük. Ebben a közelítésben már igen sok értékes eredmény látott napvilágot, mint amilyen például a kvarkbezárás bizonyítása és a hadrontömegek kiszámítása. A rács-QCD egy részletesebb leírását a második fejezet tartalmazza.

Értekezésemben a mezon-mezon kölcsönhatásokat tanulmányoztam egy QCD modell keretében. Pontosabban az olyan nehéz mezonok kölcsönhatá-

sát vizsgáltam, amelyek kvark-antikvark alkatrészei közül az egyik nehéz, a másik pedig könnyű. A K, D, és B mezonok ilyen típusú részecskék, amelyekben az s, c vagy b típusú kvark (antikvark) nehezebb, mint az u vagy d típusú antikvark (kvark). Ennek a modellnek az őse a H_2 molekula, amelyben a két nehéz proton terében mozog két könnyű elektron. Az ilyen nehéz mezonok egymástól mért távolsága közelítőleg azonos a nehéz alkatrészek közötti távolsággal. Ezért a meghatározandó $V(r)$ mezon-mezon potenciálban szereplő r távolságot azonosnak vehetjük a nehéz alkatrészek közti távolsággal. Ez nagyban leegyszerűsíti a számításokat. Az alkalmazott módszer újdonsága abban áll, hogy míg az eddigi, hasonló jellegű nemperturbatív többkvark-rendszer tanulmányokban az összes kvark sztatikus volt, esetünkben a könnyű alkatrészek dinamikus szabadsági fokokkal is rendelkeznek. Így lehetővé válik egy realisztikus mezon-mezon kölcsönhatási potenciál kiszámolása, amely tartalmaz olyan járulékokat is, amelyek a könnyű kvarkcseréből, valamint a gluonok és könnyű kvarkok kölcsönhatásából származnak. A fenti módon a barion-barion kölcsönhatások mikroszkópikus tárgyalása is lehetséges, de ebben az esetben a 12–pont Green-függvények kiszámítására lenne szükség, ami egyelőre meghaladja a rendelkezésünkre álló számítógépkapacitást.

Az eredményeket a harmadik fejezet tartalmazza. Első lépésként két azonos pszeudoskalár mezon közötti kölcsönhatást tanulmányoztam, meghatározva a kölcsönhatási potenciált. Ennek érdekében kiszámoltam a négykvark-rendszer időbeni fejlődését leíró 8–pont Green-függvényt. Ez a hadronok szintjén egy 4-pont mezon-mezon időkorrelátornak felel meg. Változtatva a nehéz alkatrészek távolságát meghatároztam ezen korrelátor távolságfüggését. A mezon-mezon rendszer $W(r)$ energiáját az időkorrelátor aszimptotikus viselkedéséből határoztam meg, felhasználva a kétrészecske-rendszer kvantummechanikai Green-függvényének energia sajátállapotok szerinti kifejtését. Ez az eljárás tulajdonképpen a kvantummechanikai Green-függvény meghatározásának a fordított művelete: itt a a Green-függvény ismert, amelyet a mikroszkópikus (QCD) modellben határozunk meg, és a potenciált származtatjuk le ezen Green-függvény kvantummechanikai kifejezéséből. A mezon-mezon potenciált végül a $V(r) = W(r) - 2m$ képlet adja meg, ahol $2m$ a két nemkölcsönható mezon tömege. Ezt a megszokott módon, a nehéz mezon időfejlődését leíró korrelátor aszimptotikus időfüggéséből lehet meghatározni.

A mezon- és mezon-mezon korrelátorok időfüggését nemperturbatív rács-QCD számítások segítségével határoztam meg. A szimulációkat quenched-közelítésben, Kogut-Susskind fermionformalizmusban végeztem, a könnyű

kvarktömegek egy sorozatára. Egy rövid távú, kb. 2 rácsállandónyi (fizikai egységekben kb. 0.4 fm) sugarú, vonzó jellegű ($0.04 - 0.1$ inverz rácsállandónyi, ill. $40 - 100$ MeV közötti) kölcsönhatást találtam, amely a könnyű kvarktömeg csökkenésével erősödik. Így felmerül a rezonáns mezon-mezon állapotok kialakulásának lehetősége, de vizsgálataim ilyen kvázi kötött állapotokat nem mutattak ki.

Mivel hasonló jellegű számítások idáig még nem történtek, fontos szempont volt a szimulációk során felmerülő szisztematikus hibák felmérése és kiküszöbölése. Ilyen hibák jelentkezhetnek a virtuális kvark-antikvark párkeltéssel járó járulékok elhagyása, a véges rácsállandó, ill. rácsméret, valamint a gerjesztett állapotok járulékai miatt. Vizsgálataim azt mutatják, hogy ezek a hibák esetünkben nem jelentősek.

A különböző nehéz mezon-mezon kölcsönhatások közül a kaon-antikaon ($K\bar{K}$) kölcsönhatások ismerete tűnik a legfontosabbnak. Többkvark-állapotok elméleti vizsgálatai arra utalnak, hogy kötött kétkvark-kétantikvark állapot valószínűleg csak mezon-antimezon kötött állapotként valósul meg. Elképzelhető, hogy a kvark-antikvark állapotként nem értelmezhető $a_0(980)$ és $f_0(975)$ részecskék ilyen gyengén kötött $K\bar{K}$ „molekulák". Ezen kérdések vizsgálata céljából tanulmányoztam egy nehéz mezon és az antirészecskéje közötti kölcsönhatásokat, meghatározva az $I = 0$ és $I = 1$ izospinű állapotokban a potenciál gluoncsere-járulékát, illetve a vegyértékkvarkcsere-járulékokat is kiszámolva a teljes potenciált. Minden esetben vonzó jellegű kölcsönhatást találtam, amely jóval erősebb a két azonos mezon esetén kapottnál. A pusztán gluoncserével megvalósuló kölcsönhatási potenciál nagyon rövid hatótávú (kevesebb, mint 1 rácsállandó, vagyis 0.2 fm) és mélysége $0.6 - 0.9$ inverz rácsállandó, vagyis $600 - 900$ MeV. A mezon-mezon esethez hasonlóan a vonzás a könnyű kvarktömeg csökkenésével erősödik. Az $I = 0$ állapontban a potenciál nagyobb távolságoknál a gluoncsere-potenciállal azonos, míg nagyon kis távolságoknál valamivel kisebb erősségű, mintegy 0.4 inverz rácsállandó, vagyis 400 MeV. Ezt a potenciált kísérleti szórási eredményekből meghatározott $K\bar{K}$ potenciálokkal tudtam összehasonlítani. Jó kvalitatív egyezést találtam. Az $I = 1$ állapotban a potenciál nagyobb hatótávú (mintegy 1.5 rácsállandó, vagyis 0.3 fm), ami azzal magyarázható, hogy ebben az esetben a gluoncserén kívül korrelált könnyű kvark-antikvark pár (mezon) cserék is adnak járulékot. A rezonáns állapotok kialakulásának lehetőségét a mezon-antimezon kölcsönhatások esetében is megvizsgáltam. Vizsgálataim arra utalnak, hogy sem kötött, sem rezonáns állapotok nem alakulnak ki.

A rácsszámítások területén az utóbbi évek egyik legnagyobb vívmányát

a „javított hatás” módszerének kifejlesztése jelentette. Ezek megjelenése új, eddig reménytelen messzeségben levő távlatokat nyit meg. Ilyen lehet például egy, a nukleonok kölcsönhatását leíró, minden eddiginél pontosabb rácsszimuláció is. Ez motiválta azt, hogy a számítógépes kódba beépítsem az egyik „legnépszerűbb”, a gluonhatás diszkretizációját tökéletesítő algoritmust. A fejezet utolsó előtti alfejezete tartalmazza a módszer rövid leírását, valamint a javított gluonhatással számolt mezon-mezon kölcsönhatási potenciálokat, melyek jó egyezést mutatnak a nem javított hatással számoltakkal. Ez azt mutatja, hogy esetünkben a diszkretizáció következtében megjelenő anizotrópiahibák nem jelentősek. Az utolsó fejezet tartalmazza az elért eredmények összefoglalóját, valamint néhány, a témához kapcsolódó további kutatási tervet.

Acknowledgments

First of all, I would like to thank my advisor Prof. Dr. István Lovas for his generous help during all stages of this work. Part of the work was done at the Technical University of Vienna, under the instruction of Doz. Dr. Dipl.-Ing. Harald Markum. It is a pleasure to thank him for introducing me in this project and for lots of advise during and after my stay in Vienna. I appreciate the many productive discussions with Dr. Dipl.-Ing. Klaus Rabitsch, Prof. Dr. Rudolf Fiebig, Prof. Dr. János Polónyi, Doz. Dr. Kornél Sailer, Dr. Zsolt Schram, MSc. Béla Iványi, Dr. Dipl.-Ing. Jürgen Riedler and Dipl.-Ing. Christian Starkjohann. Besides the PhD scholarship financed by the Hungarian Ministry of Science and Education (MKM), the money of the Hungarian National Scientific Research Fund (OTKA) from the projects T-016249 and T-023844, and that of the Research Group in Physics of the Hungarian Academy of Science, Debrecen helped me to survive. The stay in Vienna was financed by the TEMPUS program under JEP No. 7202/1994. Last but not least I would like to thank the staff of the Department of Theoretical Physics of Kossuth Lajos University, especially Prof. Dr. István Lovas and Doz. Dr. Kornél Sailer for making me feel "at home" during my stay in Debrecen.

Bibliography

[1] L. Eisenbud and E.P. Wigner, Proc. Nat. Acad. Sci. U. S. 27 (1941) 281.

[2] S. Okubo and R. Marshak, Ann. Phys. 4 (1985) 166.

[3] R. V. Reid, Ann. Phys. (N.Y.) 50 (1968) 411.

[4] K. Holinde, Phys. Rep. 68 (1981) 121.

[5] R. Machleidt, K. Holinde, and Ch. Elster, Phys. Rep. 149 (1987) 1.

[6] R. Machleidt, Advances in Nucl. Phys. 19, Plenum (New York, 1989) 189.

[7] M. Lacombe, B. Loiseau, R. Vinh Mau, J. Côté, P. Pirès, and R. de Tourreil, Phys. Rev. C23 (1981) 2405.

[8] N. Isgur, in "The New Aspects of Subnuclear Physics", Plenum (New York, 1980).

[9] C. DeTar, Phys. Rev. D17 (1978) 302.

[10] A. Chodos, R. L. Jaffe, K. Johnson, C. B. Thorn, and V. F. Weisskopf, Phys. Rev. D9 (1974) 3471.

[11] G. E. Brown and M. Rho, Phys. Lett. B82 (1979) 177.

[12] A. W. Thomas, Advances in Nucl. Phys. 13 (1983) 1.

[13] G. t'Hooft, unpublished comments at the conference in Marseille (1972).

[14] H.D. Politzer, Phys. Rev. Lett. 30 (1973) 1346.

[15] K. G. Wilson, Phys. Rev. D10 (1974) 2445.

[16] M. Creutz, "Quarks, Gluons and Lattices", Cambridge University Press (Cambridge, 1983).

[17] H.J. Rothe, "Lattice Gauge Theories, An Introduction", World Scientific (Singapore, 1992).

[18] I. Montvay and G. Münster, "Quantum Fields on a Lattice", Cambridge University Press (Cambridge, 1994).

[19] D. G. Richards, D. K. Sinclair, and D. Sivers, Phys. Rev. D42 (1990) 3191.

[20] see A.M. Green and P. Pennanen, Phys. Lett. B426 (1998) 243, and references therein.

[21] K. Rabitsch, H. Markum, and W. Sakuler, Phys. Lett. B318 (1993) 507.

[22] M. Fukugita, Y. Kuramashi, M. Okawa, H. Mino, and A. Ukawa, Phys. Rev. D52 (1995) 3003.

[23] R.P. Feynman, Rev. Mod. Phys. 20 (1948) 367.

[24] R. P. Feynman and A. R. Hibbs, "Quantum Mechanics and Path Integrals", McGraw-Hill (New York 1965).

[25] A. Hasenfratz and P. Hasenfratz, Ann. Rev. Nucl. Part. Sci. 35 (1985) 559.

[26] L. H. Karsten and J. Smit, Nucl. Phys. B183 (1981) 103.

[27] H. B. Nielson and M. Ninomiya, Nucl. Phys. B185 (1981) 20.

[28] J. Kogut and L. Susskind, Phys. Rev. D11 (1975) 395.

[29] L. Susskind, Phys. Rev. D16 (1977) 3031.

[30] S. Okubo, Phys. Lett. 5 (1963) 165; G. Zweig, CERN preprint TH 401, 412 (1964); J. Iizuka, Prog. Theor. Phys. Suppl. 37 (1966) 21.

[31] G. Veneziano, Nuovo Cim. 57A (1968) 190.

[32] H. Hamber and G. Parisi, Phys. Rev. Lett. 47 (1981) 1792.

[33] D. Weingarten, Phys. Lett. 109B (1982) 57.

[34] S. Gottlieb, W. Liu, D. Toussaint, R. L. Renken, and R. L. Sugar, Phys. Rev. D35 (1987) 2531.

[35] R. T. Scalettar, D. J. Scalapino, and R. L. Sugar, Phys. Rev. B34 (1986) 7911.

[36] P. Rossi, C.T.H. Davies, and G.P. Lepage, Nucl. Phys. B297 (1988) 287.

[37] M.R. Hestenes and E. Stiefel, Nat. Bur. Standards J. Res. 49 (1952) 409.

[38] J.D. Canosa and H. R. Fiebig, Nucl. Phys. B (Proc. Suppl.) 34 (1994) 561.

[39] J.D. Canosa, H. R. Fiebig, and H. Markum, Nucl. Phys. B (Proc. Suppl.) 42 (1995) 657.

[40] H.R. Fiebig, O. Linsuain, H. Markum, and K. Rabitsch, Nucl. Phys. B (Proc. Suppl.) 47 (1996) 695.

[41] H.R. Fiebig, O. Linsuain, H. Markum and K. Rabitsch, Phys. Lett. B386 (1996) 285.

[42] J.D. Canosa and H.R. Fiebig, Phys. Rev. D55 (1997) 1487.

[43] A. Mihály, H.R. Fiebig, H. Markum, and K. Rabitsch, Proceedings of "Hadron Structure '96", Slovac Academy of Science (Bratislava, 1996) 172.

[44] H.R. Fiebig, H. Markum, A. Mihály, K. Rabitsch, W. Sakuler, and C. Starkjohann, Nucl. Phys. B (Proc. Suppl.) 47 (1996) 394.

[45] A. Mihály, H.R. Fiebig, H. Markum, and K. Rabitsch, Phys. Rev. D55 (1997) 3077.

[46] H.R. Fiebig, H. Markum, A. Mihály, and K. Rabitsch, Nucl. Phys. B (Proc. Suppl.) 53 (1997) 804.

[47] H.R. Fiebig, H. Markum, A. Mihály and K. Rabitsch, Nucl. Phys. B (Proc. Suppl.) 63A-C (1998) 386.

[48] N. Kawamoto and J. Smit, Nucl. Phys. B192 (1981) 100.

[49] H. Klugberg-Stern, A. Morel, O. Napoly and B. Petersson, Nucl. Phys. B220 (1983) 447.

[50] G.W. Kilcup and S.R. Sharpe, Nucl. Phys. B283 (1987) 493.

[51] K. Rabitsch, "Hadron-Hadron Potentials from Lattice Quantum Chromodynamics", Doctoral Thesis, Vienna University of Technology (1997).

[52] W. Lucha, F.F. Schöberl, and D. Gromes, Phys. Rep. 200 (1991) 127.

[53] D. Barkai, K.J.M. Moriarty, and C. Rebbi, Phys. Lett. B156 (1985) 385.

[54] W.H. Press, S.A. Teukolsky, W.T. Vetterling, and B.P. Flannery, "Numerical Recipes in Fortran", Cambridge University Press, 2nd Edition (Cambridge, 1992) 675.

[55] F. Fucito, E. Marinari, G. Parisi, and C. Rebbi, Nucl. Phys. B180[FS2] (1981) 369.

[56] Particle Data Group: R. M. Barnett *et al.*, Phys. Rev. D54 (1996) 1.

[57] J. Sexton, A. Vaccarino, and D. Weingarten, Phys. Rev. Lett. 75 (1995) 4563; Nucl. Phys. B (Proc. Suppl.) 53 (1997) 232.

[58] G. Bali *et al.*, Phys. Lett. B309 (1993) 378.

[59] C. Bernard *et al.*, Nucl. Phys. B (Proc. Suppl.) 53 (1997) 228; C. Bernard *et al.*, Phys. Rev. D56 (1997) 7039.

[60] C. Michael and J. Peisa, Nucl. Phys. B (Proc. Suppl.) 63A-C (1998) 55.

[61] D.B. Lichtenberg, R. Roncaglia, and E. Predazzi, Proceedings of the International Workshop, Diquarks 3, Torino, hep-ph/9611428.

[62] T. Vertse, K.F. Pál and Z. Balogh, Comp. Phys. Comm. 27 (1982) 309.

[63] J. Weinstein and N. Isgur, Phys. Rev. Lett. 48 (1982) 659.

[64] J. Weinstein and N. Isgur, Phys. Rev. D41 (1990) 2236.

[65] M. Sander, "Quanteninversion und Hadron-Hadron Wechselwirkungen", PhD. Thesis, University of Hamburg, Shaker (Aachen 1997).

[66] H.R. Fiebig, H. Markum, A. Mihály, K. Rabitsch, M. Sander, and H. V. von Geramb, in preparation.

[67] K. Königsmann, preprint CERN-PPE/93-182.

[68] K. Karch *et al.* Z. Phys. C54 (1992) 33.

[69] R. Kaminski, L. Lesniak, and J.P. Maillet, Phys. Rev. D50 (1994) 3145.

[70] K. Chadan and P.C. Sabatier, "Inverse Problems in Quantum Scattering Theory", 2nd Edition, Springer (Berlin, 1989);

[71] H.V. von Geramb (ed.), "Quantum Inversion Theory and Applications", Lect. Notes in Phys. 427, Springer (1994).

[72] R. Kaminski and L. Lesniak, Phys. Rev. C51 (1995) 2264.

[73] T. DeGrand, A. Hasenfratz, P. Hasenfratz, and F. Niedermayer, Nucl. Phys. B454 (1995) 587; Nucl. Phys. B454 (1995) 615.

[74] M. Alford, W. Dimm, G.P. Lepage, G. Hockney and P.B. Mackenzie, Nucl. Phys. B (Proc. Suppl.) 42 (1995) 787; Phys. Lett. B361 (1995) 87.

[75] K. Symanzik, Nucl. Phys. B226 (1983) 187.

[76] G.P. Lepage and P.B. Mackenzie, Phys. Rev. D48 (1993) 2250.

[77] G. Gurci, P. Menotti, and G. Pafutti, Phys. Lett. 130B (1983) 205, Erratum: *ibid.* 135B (1984) 516.

[78] M. Lüscher and P. Weisz, Comm. Math. Phys. 97 (1985) 59.

[79] P. Weisz and R. Wohlert, Nucl. Phys. B236 (1984) 397.

[80] S. Sharpe, Nucl. Phys. B (Proc. Suppl.) 34 (1994) 403.

[81] S. Naik, Nucl. Phys. B316 (1989) 238.

[82] Y. Luo, Phys. Rev. D57 (1998) 265

[83] H.R. Fiebig, H. Markum, A. Mihály, K. Rabitsch, and R.M. Woloshyn, Nucl. Phys. B (Proc. Suppl.) 63A-C (1998) 188.

[84] C. Stewart and R. Koniuk, hep-lat/9803003, to appear in Phys. Rev. D.

[85] P.B. Mackenzie and H.B. Thacker, Phys. Rev. Lett. 23 (1985) 2539.

[86] Y.T. Iwasaki, T. Yoshie, and Y. Tsuboi, Phys. Rev. Lett. 60 (1988) 1371.

Documentation of Publications

1. H.R. Fiebig, H. Markum, A. Mihály, K. Rabitsch, W. Sakuler and C. Starkjohann: *Meson-meson interactions – from static to dynamic valence quarks*, Nucl. Phys. B (Proc. Suppl.) 47 (1996) 394, hep-lat/9510032.

2. A. Mihály, H.R. Fiebig, H. Markum and K. Rabitsch: *Potentials between heavy-light mesons on the lattice*, Proceedings of "Hadron Structure '96", Slovac Academy of Science (Bratislava, 1996) 172.

3. A. Mihály, H.R. Fiebig, H. Markum and K. Rabitsch: *Interactions between heavy-light mesons in lattice QCD*, Phys. Rev. D55 (1997) 3077.

4. H.R. Fiebig, H. Markum, A. Mihály and K. Rabitsch, *Forces between composite particles in QCD*, Nucl. Phys. B (Proc. Suppl.) 53 (1997) 804, hep-lat/9608065.

5. H.R. Fiebig, H. Markum, A. Mihály and K. Rabitsch, *Potentials between heavy-light mesons from lattice and inverse scattering theory*, Nucl. Phys. B (Proc. Suppl.) 63A-C (1998) 386, hep-lat/9709150.

6. H.R. Fiebig, H. Markum, A. Mihály, K. Rabitsch and R.M. Woloshyn, *Two-body spectra of pseudoscalar mesons with an $O(a^2)$–improved lattice action using Wilson fermions*, Nucl. Phys. B (Proc. Suppl.) 63A-C (1998) 188, hep-lat/9709152.

7. H.R. Fiebig, H. Markum, A. Mihály and K. Rabitsch, *Potentials between pion-like particles from lattice QCD*, in preparation

8. H.R. Fiebig, H. Markum, A. Mihály and K. Rabitsch, *On the $I = 2$ channel π–π interaction in the chiral limit*, to appear in Nucl. Phys. B (Proc. Suppl.).

9. A. Mihály, H.R. Fiebig, H. Markum and K. Rabitsch, *$M\bar{M}$ interactions in different isospin channels within lattice QCD*, in preparation.

10. H.R. Fiebig, H. Markum, A. Mihály, K. Rabitsch, M. Sander, and H. V. von Geramb, *Meson–meson potentials from lattice QCD and inverse scattering*, in preparation.

Lectures, Seminars, Talks and Posters:

1. *Fermionok szimulációja rácson (Simulating fermions on the lattice)*, theory seminar, Debrecen, 09/94

2. *Hadronok közötti kölcsönhatás a kvantumszíndinamikában (Interactions between hadrons in QCD)*, theory seminar, Debrecen, 02/96

3. *Meson-meson potentials with improved action in lattice QCD*, talk at the XXXV. Internationale Universitätswochen für Kern- und Teilchenphysik, Schladming, Austria, 03/96

4. *Hadron-hadron interactions within lattice QCD*, talk at the DPG-Frühjahrstagung, Physik der Hadronen und Kerne, Stuttgart, 03/96

5. *A comparison of potentials between heavy-light mesons from lattice QCD and inverse scattering theory*, talk at the 6th Workshop on Lattice Field Theory, Vienna, 09/96

6. *Javított szimuláció a QCD-ben (Improved simulation method in QCD)*, talk at the Workshop on Computer Simulations and Informatics, Debrecen, 09/96

7. *Lattice-QCD studies of meson-meson interactions with dynamic quark propagators*, talk at the 12th Nordic Meeting, Gräftåvallen, Sweden, 01/97

8. *Improved action and hadron-hadron interactions*, lecture series at the Graduate School on Quantum Field Theory, Debrecen, 09/97

9. *Interactions between heavy-light mesons*, poster at the 5th Workshop on Lattice Field Theory, Vienna, 05/95

10. *Potentials between heavy-light mesons from lattice and inverse scattering theory*, poster at the XV International Symposium on Lattice Field Theory, Edinburgh, 07/97

11. *Meson-meson interaction with Kogut-Susskind fermions*, poster at the 7th Workshop on Lattice Field Theory, Vienna, 09/97